LOW-VELOCITY IMPACT BEHAVIOUR OF GREEN EPOXY BIOCOMPOSITE LAMINATES REINFORCED BY SISAL FIBERS

C. Militello[a], F. Bongiorno[a], G. Epasto[b], B. Zuccarello[a]

[a] *Università degli Studi di Palermo - Dipartimento di Ingegneria, Viale delle Scienze, 90128 Palermo, e-mail: carmelo.militello01@unipa.it, francesco.bongiorno01@unipa.it, bernardo.zuccarello@unipa.it*

[b] *Università degli Studi di Messina - Dipartimento di Ingegneria, Contrada di Dio, Sant'Agata 98166 Messina, e-mail: gabriella.epasto@unime.it*

Abstract

Due to its good mechanical characteristics, low cost and high availability in the current market, sisal fiber is one of the most used for the manufacturing of non-structural eco-friendly components in various industrial fields (automotive, marine, civil construction etc.) although recently, as it was expected, its use has been proposed also for the implementation of high performance biocomposites laminates to be employed for structural applications. The particular sub-fibrillar structure of the sisal fiber (similar to aramid fibers) and the corresponding anisotropic behaviour detected by recent research activities, suggest that such biocomposites should exhibit also high impact strenght, in such a way to permit its advantageously use also for the manufacturing of crashworthy components (bumpers, helmets, protection systems for operating machines etc.), that are at the same time also eco-friendly, lightweight and cheap. Through a low-velocity impact tests campaign, integrated by computer tomography (CT) and carried out on various "green epoxy"/sisal biocomposites laminates, by varying the main influence parameters such as reinforcement distribution, fiber volume fraction and laminate lay-up, it has been detected that angle-ply laminates with high fiber volume fraction exhibits specific impact performances superior to those of biocomposites reinforced by other natural fibers (flax, hemp, jute, ramie etc.), and comparable with those of the best composites specially reported in literature, so that they can be actually used to substitute the synthetic materials for the manufacture of interesting eco-friendly energy absorbing devices, that are also lighter and cheaper.

Keywords: Biocomposites, natural fibers, sisal, impact strength, computed tomography.

1. INTRODUTION

The use of natural fibers (flax, hemp, jute, sisal, ramie, coconut, etc.) for the manufacturing of innovative biocomposites characterized by good mechanical performance, lightweight and low cost is very successful, has widely corroborating by the high number of review articles published recently [1-

22]; when combined with proper eco-friendly and/or renewable biopolymers, they allow to obtain interesting completely renewable biocomposites, compostable or biodegradable.

These fibers generally have good mechanical properties, good acoustic and thermal insulation, combined with low damage during biocomposite manufacturing and easy workability. Moreover, they are characterized by low specific weight and low cost (both always less than those of the synthetic fibers) so that, unlike synthetic fibers, their application for the reinforcement of biopolymers allows not only to improve their mechanical performance, but also to reduce weight and cost of the final components. For these reasons, biocomposites are currently very attractive in different industrial fields (automotive, marine , civil construction, etc.) for non-structural applications, although recently several research works have also been addressed to the development of high performance biocomposites that can be used for structural applications. In more detail, various studies have also been carried out to improve the mechanical characteristics of biocomposites: from the development of suitable fiber treatments [23-31] mainly aimed to the improvement of the fiber-matrix adhesion, to the use of fillers able to increase the mechanical characteristic of the fibers [32, 33], to the experimentation of hybrid biocomposites obtained by the combination of different types of natural fibers [34-36] or the mixture of natural and synthetic fibers [37].

Among the various natural fibers used for the manufacturing of biocomposites, particularly interesting is the agave sisalana fibre (sisal), characterized by short replacement times, high availability in the current market, possibility of cultivation on marginal soils, but also good stiffness and mechanical strength combined with low cost and good compatibility with many polymeric matrixes [38-60]. Also, the intimate fibrillar structure makes it the natural fiber with the highest hardness, comparable with that of the fiberglass; the close similarity to the aramid fibres (kevlar, etc.) makes think to a good behaviour to the impact and fracture and, consequently, to its advantageous use for the manufacturing of innovative energy absorbing devices in various field of the industrial production as automotive, shipbuilding, earth-moving machines etc. However, these properties have not yet been clearly demonstrated, as the most literature works, have mainly concerned the evaluation of the static mechanical properties of these biocomposites.

Several studies are available in the literature on the evaluation of the response to impact of composites laminates [61-99], and various research works have considered biocomposites and hybrid biocomposites reinforced by natural fibers [61-81], among which the most studied one has been the flax fibre.

In particular, in [63] Wang et al. have analysed the influence of the laminate thickness in the impact response of epoxy biocomposites reinforced by flax fibres, showing a simple linear relationship between specimens thickness and impact strength (energy absorption capabilities).

In [64], Al-hajaj et al. have carried out the first experimental investigations on new carbon/flax hybrid composites for impact damage assessment; such hybrid composites have been found to exhibit better penetration strength than only flax reinforced biocomposites.

In [65] Sarasini et al. have demonstrated that the greater ductility of basalt fibers compared to carbon fibres, allows the user to obtain hybrid composites with greater global strain, increased surface damaging and improved energy absorption capability; in [66] the same authors also considered carbon/flax hybrid composites.

In [69], by analyzing ternary hybrid composites reinforced by flax/basalt/carbon with epoxy matrix, Nisini et al. have demonstrated how impact loading give rises to significant delamination at the interface between the flax and basalt layers. It has been also detected the significant influence of the laminate lay-up on the impact fracture growth patterns.

In [81], Al-Maharma et al. have highlighted the mutual correlation between the main factors influencing fracture and impact strength of biocomposites. In particular, they pointed out that a weak fiber/matrix adhesion corresponds to a great capability to dissipate impacting energy through pull-out damage mechanisms. However, this capability varies significantly with type, distribution and volume concentration of the fiber, whereas it is in general only slight influenced by the peculiar matrix properties [82].

In [90] by considering glass fiber composites, Evci et al. have shown that the choice of the type of fabric used as reinforcement in polymeric composites influences significantly the impact behaviour. In particular, they have observed how composites reinforced by unidirectional stitched fabrics, although exhibit higher static strength, in terms of impact strength they are less performing than composites reinforced by woven fabrics.

In [91] through numerical analysis of the impact damage mechanisms of carbon composites with different helical lay-up, Jiang et al. have shown that a greater angle of rotation between the laminae increases the cracking path of the matrix and thus the impact strength.

In [92-95] the authors have shown how the post-impact evaluation of the internal damage phenomena as well as of the fracture mechanisms of composites, can be accurately carried out by non-destructive techniques, such as computed tomography (TC) [100-102], thermography [103] and ultrasonic techniques.

Despite the interesting dynamic performance expected from biocomposites reinforced by agave fibres, to date none systematic study of the impact behaviour of such materials has yet been carried out. Therefore, in order to give a contribution in this regard, through drop-weight low-velocity impact tests the present work performs a detailed analysis of the impact behaviour of biocomposites reinforced by agave fibers by varying the main influence parameters, such as fiber distribution (random, unidirectional), volume concentration and lay-up (unidirectional, cross-ply, quasi-isotropic). Also, the damage mechanisms and the collapse processes of the specimens subjected to impact tests is analysed in detail by using high resolution computed tomography (CT). Finally, accurate analyses of the results are performed in order to implement reliable models that can be used to predict the impact behaviour at the design stage.

2. MATERIALS: REINFORCEMENT FIBER AND MATRIX

2.1 Reinforcement fiber

The sisal fibers used for the manufacturing of the biocomposites considered in the present research work, are the so called structural fibers that can be considered a completely renewable material because they are not submitted to any chemical treatment. Before their use for the biocomposite manufacturing they have been only subjected to a simple drying process accomplished by using an electrical resistance oven, at a controlled temperature of 75 °C for about 1 hour.

Tab. 1 shows the density ρ_f of the selected fibers and the relative longitudinal mechanical properties as the tensile strength $\sigma_{L,R}^{(f)}$, tensile Young modulus $E_L^{(f)}$ and the failure strain $\varepsilon_{L,R}^{(f)}$ determined by proper single-fiber tensile tests [104]. Noteworthy the optimal value of the longitudinal failure strain, equal to 1.75%, that for a good quality composite has to take values lower than the failure strain of the matrix; as it is well known in the mechanics of composites, such a condition avoids significance limitations of the mechanical strength due to failure phenomena of the matrix with consequent premature composite failure associated with matrix micro-cracking and/or fiber/matrix debonding.

2.2 Matrix

The matrix used for the manufacturing of the biocomposites, is a green epoxy resin called SUPERSAP CNR (with IHN hardener) and produced by Entropy Resin Inc. (CA), USA. As it has been shown in previous studies of the same authors [51-60], such a resin has good mechanical characteristics, synthetically reported in Tab.2. In detail, it exhibits a strain failure value higher than that of the sisal fibers considered (see Tab.1), so that it allows to obtain good quality biocomposites.

3. BIOCOMPOSITE MANUFACTURING

The biocomposites have been proper manufactured by using a unidirectional *stitched* fabric and a MAT type (discontinuous fiber randomly oriented) fabric, both purposely implemented in laboratory.

In more detail, unidirectional fabrics having a specific weight of 225 g/m^2 with orientation of 0° (Fig.1a) and 45° (Fig.1b), has been obtained by the manual stretching of the fibers (to eliminate the natural fiber undulations), the successive accurate mutual alignment by placing them in parallel bundles, and a final stitching by using an automatic sewing machine.

MAT fabrics with specific weight of 255 g/m^2 (Fig.1c), have been manufactured by placing randomly discontinuous fibers (length of 60÷70 mm) properly pre-impregnated by spraying the same green epoxy resin with a suitable compressed air device.

By using these fabrics, various laminates have been manufactured by hand lay-up followed by an optimized "*compression moulding*" process [51-60], carried out through a plane mould of 260 x 260 mm, and a hydraulic press of 100 tons. In order to optimize the quality of the laminates, successively

they have been subjected to a suitable curing process accomplished by using an electrical resistance oven, at a controlled temperature of 80 °C for about 120 min.

In Tab.3 the various types of laminates so obtained are listed (all having thickness of 3.5 mm), along with the corresponding fiber volume fraction V_f and lay-up. In particular, three different long fiber lay-up have been manufactured: unidirectional (UD), cross-ply (CP) and quasi-isotropic (QI); for each lay-up three different fiber volume fractions have been considered: V_f = 35%, 50% and 70%. Also, by using the MAT fabrics, three laminates having V_f = 15%, 30% and 35%, have been obtained (as it is well known the random fiber distribution allows to obtain good quality laminates only with V_f values less than 30-35%).

From each laminate, rectangular (25 x 260 mm) specimens for tensile tests and square (60 x 60 mm) specimens for low-velocity impact tests (see Fig.2), have been cut by using a *Proxxon* type circular saw.

4. EXPERIMENTAL TESTS

4.1 Static tensile tests

The various biocomposite laminates have been first characterized by tensile tests, carried out by using a servo-hydraulic material test machine type MTS 810, instrumented by an MTS extensometer having a measuring base of 25 mm. The tests have been performed in accordance with the ASTM standard D3039/D D3039M [105]. For each biocomposite laminate considered, the following Tab.4 shows the detected mean values of tensile strength $\sigma_{L,R}$, failure strain $\varepsilon_{L,R}$ and tensile Young modulus E_L (values that are not dependent on the load direction for QI and MAT laminates). From Tab.4 it is observed how the tensile characteristics of UD, CP and QI laminates obey to the rule of mixture (ROM), i.e. they increase almost linearly with V_f. In more detail, the UD biocomposites exhibit a maximum tensile strength of 471.4 MPa for V_f = 70%, value that is significantly higher than that of the other CP (275.3 MPa) and QI (161.5 MPa) configurations examined. In other words, cross-ply and quasi-isotropic laminates have a tensile strength respectively of about 65% and 35% of the unidirectional one. Noteworthy is that, unlike previous laminates, the tensile strength of the MAT laminates is a non-monotonic function of V_f, with a maximum absolute value of 51.2 MPa (slightly higher than that of the matrix alone) for V_f = 30 % [51].

4.2 Impact tests

The impact characterization of the biocomposites considered, have been carried out by "*drop-weight*" tests, i.e. through low-velocity impact tests. In detail, the impact tests have been performed by using a *Ceast Fractovis Plus* (see Fig.3a,b) test machine, equipped with a special system that allows to eliminate possible multiple impacts. The machine is equipped by an impactor having a hemispherical

tip with a nominal diameter of 20 mm (Fig.3b,c). During the tests, the specimens have been simply supported on a rigid metallic ring (Fig.3b,c) having an internal diameter of 40 mm.

For each type of biocomposite laminate considered, the impact tests have been performed by using an impacting mass of 6.5 kg and different values of the impact energy E_i have been obtained by varying properly its initial drop height. In particular, for each type of biocomposite the tests have been carried out by increasing the impact energy until the complete penetration of the whole specimen was observed; in practice, impact energies ranging from 5 to 30 J, with corresponding impact velocity ranging from about 1.25 to 3.00 m/s, have been used. By using samples consisting of 3 specimens for each examined biocomposite, about 100 impact tests have been performed at all.

The test machine provides the impact force $F_i(t)$ that the striker applies to the specimen during the test, and its corresponding displacement s measured from the initial impact position; from such measurements the total energy E_a absorbed by the specimen and the possible elastic return energy $E_{e,r}$, can be immediately computed by integrating the force-displacement curve $F_i(s)$, whose characteristics are generally strictly related to the particular material examined.

In order to examine such particular characteristics, Fig.4 shows the results in terms of the $F_i(t)$ and $F_i(s)$ curves provided by the impact test of the QI biocomposite laminate having V_f = 35%, carried out by using a relatively low impact energy E_i = 10 J, which causes only a partial damage of the laminate.

In detail, from the force-time curve $F_i(t)$ (see Fig.4a) it is possible to identify three characteristic parameters such as: 1) the first impact damage force F_i^{FID}, which corresponds to the point of the curve where the first abrupt load reduction with subsequent restart occurs, 2) the peak force or maximum impact force F_i^{MAX} and 3) the force of the monotone load reduction F_i^{MLR}, which corresponds to the point from which the curve becomes decreasing in a monotonic way. In case of partial damage of the examined specimens (absence of complete perforation), as it is the examined case, this last characteristic point corresponds in practice to the start point of the elastic return. Therefore, in the diagram of the $F_i(t)$ curve it is possible to identify four different zones: zone I included between the origin and the first impact damage force F_i^{FID}, corresponding to the elastic behaviour of the material, zone II included between F_i^{FID} and F_i^{MAX}, corresponding to the progressive elasto-plastic damage until the maximum force is reached, zone III included between F_i^{MAX} and F_i^{MLR}, corresponding to the successive elasto-plastic damage after F_i^{MAX} is reached, and zone IV beyond F_i^{MLR}, which corresponds to the elastic return of the specimen.

It is important to observe how in this case (QI specimens) the deviation from the linear behaviour occurs for a relatively high impact force level, equal to about 85-90% of the maximum load.

These characteristic force values and the relative zones above defined, can also be detected in the diagram of the $F_i(s)$ curve reported in Fig.4b, whose areas correspond to characteristic energy values. First of all, it is to be noted how in the examined case of partial damage, the diagram has a characteristic closed shape, and the closed integral represents the total energy E_a absorbed by the

specimen, that is the energy dissipated through the peculiar damaging mechanisms. In particular, the area corresponding to the zone I represents the energy $E_{a,e}$ absorbed by the specimen in the elastic phase, the area corresponding to the zones II+III represents the energy $E_{a,p}$ absorbed through elasto-plastic damaging processes, whereas the area corresponding to the zone IV represents the energy $E_{e,r}$ associated to the elastic return of the specimen. In quantitative terms, the energy $E_{a,e}$ absorbed in the elastic phase is equal to about 25% of the impact energy, the energy $E_{a,p}$ absorbed in the elasto-plastic phase is equal to about 50% of the impact energy (about twice the elastic one), whereas the energy $E_{e,r}$ that characterizes the elastic return of the specimen, is also about 25% of the impact energy. Therefore, the total energy absorption E_a (about 7.5 J) is equal to the 75% of the impact energy (10 J).
In case of complete damage of the specimen (striker pierces the whole specimen) the trends of the diagrams of $F_i(t)$ and $F_i(s)$ differ from those above shown in Fig.4a and 4b; in this case, in fact, the elastic return became negligible or null and F_i^{MAX} coincides in practice with F_i^{MLR}, as it is shown, as an example, in Fig.5 that describes the results relative to the impact test of the CP biocomposite laminate having V_f = 35% and subjecting to an impact energy E_i = 20 J. In this case, only the first three phases are observed (phase IV does not exist) and the phase III is characterized by a curve $F_i(s)$ tending to zero for the maximum s value (total perforation). Obviously, in this case of complete penetration, the total energy absorbed by the specimen (about 16.1 J), corresponding to the total area under the $F_i(s)$ curve, represents the impact strength E_s of the specimen (less than the impact energy E_i =20 J). It is important to note how, unlike the previous case of QI laminate, in the case of CP laminate the value of the first damage force is relatively low (F_i^{FID} =1175 N) with respect to the maximum load (F_i^{MAX} ≈2140 N), i.e. $F_i^{FID} \approx 0.5\ F_i^{MAX}$; as it will see in the following, such a result indicates the premature delamination of the CP laminates respect to the QI laminates, due to the higher mean angular deviation between successive laminae.

5. ANALYSIS OF RESULTS AND DAMAGE EVALUATION

The results of the impact tests carried out by varying the lay-up of the laminate, the fibre volume fraction and the impact energy, are synthetically shown in Figs.6 and 7. A detailed analysis of such results for each laminate type, is reported in the following sections.

5.1 UD laminates

The three different unidirectional biocomposite laminates considered with V_f = 35%, 50% and 70%, have been tested with 3 distinct levels of impact energy E_i = 5 J, 7 J and 10 J. Figs.6a and 6b show the images after the impact test of the specimens having V_f =35% and 70% respectively. Qualitatively similar results have been obtained for specimens with V_f = 50% which, for simplicity sake, are not shown in Fig.6. From these images, it can be observed how although for low impact energies the damage consists into the classical surface indentation whose area S_D increases with the impacting

energy, for any V_f value the complete failure of the UD specimens occurs always for an impact energy E_i = 10 J and it is always associated with a particular damage mechanism that does not give rise to the classic perforation but to a typical "transverse" failure with fracture surface parallel to the fibers direction; in detail such fracture surface involves both the matrix, that collapses by transversal tensile, and the fibers that failures by transversal splitting [106].

The analysis of the characteristic curves $F_i(t)$ and $F_i(s)$ shown respectively in Figs.7a and 7b, as well as of the corresponding numerical values of F_i^{FID}, F_i^{MAX}, E_s, $E_{a,p}$ and $E_{a,e}$ reported in Tab.5, shows how the peak force is subject to a slight decrease when V_f increase; more significant is instead the decrease of the first impact damage F_i^{FID}: about -15% moving from V_f=35% to V_f=70%. However, the highest reduction (of about -30%) regards the energy $E_{a,e}$ absorbed in the elastic phase: from 2.7 J for V_f=35% to 1.9 J for V_f =70%. Such phenomena are evidently related to the brittle tensile failure of the thermosetting matrix due to the bending effects associated to the impact, as well as to the low transversal strength of the sisal fibers due to the typical transversal splitting [106]. However, the impact strength E_s increases appreciably (of about 33%) with V_f, moving from 7.3 J for V_f=35% to 9.7 J for V_f=70%, indicating clearly that, although the transversal mechanical strength decreases with V_f because the transversal strength of the fiber is lower than the matrix one [106], the specific energy associated with the splitting of the fibers is instead significantly superior to that associated to the tensile failure of the matrix.

Taking into account the above mentioned damage processes of matrix and fibers, by using the representative volume element (RVE) of the Periodic Microstructure Model (PMM) [107] schematically reported in Fig.8a, it is possible to correlate the impact strength E_s with the energy $E_f^{(sp)}$ absorbed by the fibres during the splitting damaging and the energy $E_m^{(te)}$ absorbed by matrix during the tensile damaging by the following simple energy-balance relationship:

$$E_s = E_f^{(sp)}\ 2\sqrt{\frac{V_f}{\pi}} + E_m^{(te)}\left(1 - 2\sqrt{\frac{V_f}{\pi}}\right) \qquad (1)$$

Fig.8b shows the curve obtained by fitting the values of E_s detected experimentally (see Tab.5) by Eq.1; it is possible to observe a very good accordance between the PMM model and the experimental evidence (deviations less than 5%). Moreover, the analytical expression of the fitted curve computed for V_f= 0 and V_f= π/4 provides immediately the unknown value of $E_f^{(sp)}$ and $E_m^{(te)}$ as:

$$E_f^{(sp)} = 9.84\ J; \qquad E_m^{(te)} = 1.79\ J$$

These values show that, as qualitatively expected due to the intimate sub-fibrillar structure of the sisal fibre [106] and the brittle behaviour of the thermosetting resins, the impact strength of the fibre is about 5 times higher than that of the epoxy matrix. Consequently, unlike various composites reinforced by synthetic fibres, the impact strength of the examined unidirectional biocomposites

increases significantly with the fibre volume fraction, as occurs for the longitudinal static strength too. It is possible therefore to observe that although for "transversal tensile failure" the static splitting strength of the fibres is significantly lower than the tensile strength of the matrix [106], in terms of energy absorbed under impact loading, the scenery reverses, fully confirming the high impact strength expected for the sisal fibres and, consequently, for the corresponding biocomposites, thanks to the high energy absorption associated to the fiber splitting.

5.2 CP laminates

The impact tests carried out on cross-ply biocomposite laminates have shown that for V_f =35% the complete penetration (perforation) is obtained by using an impact energy E_i =20 J, whereas for V_f =50% and V_f =70% it is obtained for E_i = 25 J and 30 J respectively (see Figs.6c and 6d concerning the two extreme V_f =35% and 70% cases). As it can be observed from the "back" face of Figs.6c and 6d, for these laminates the perforation involves fibre failure by longitudinal tensile and matrix collapse by shear stresses associated with interlaminar delamination. In detail, the experimental evidence shows that the damaged zone of the "front" surface has the circular shape of the impactor with diameter that tend to that of the impactor when the penetration tends to the complete perforation. Very different appears instead the damage of the "back" surface that exhibits an irregular shape with dimension superior to the diameter of the impactor; also, it is typically characterized by significant interlaminar delamination phenomena.

In more detail, the analysis of the impact curves (see Fig.6c and 6d) and of the numerical values reported in Tab.5 shows that, unlike previous unidirectional case, the first impact damage force and the peak force increase appreciably with V_f. In particular, by moving from V_f =35% to V_f =70% F_i^{FID} and F_i^{MAX} increase of about 140% and 66% respectively. Also, the absorbed elastic energy $E_{a,e}$ is subjected to significant increments (+550%) by passing from 1.2 J to 7.8 J, whereas the impact strength E_s increases from 16.1 J to 29.9 J (about +85%), with increments almost directly proportional to V_f.

Taking into account the main damaging processes (longitudinal tensile failure of the fibers and delamination failure of the matrix) it is possible to write that the impact strength E_s of the CP biocomposites examined, is given by the simple average weight of the energy $E_f^{(te)}$ absorbed by the fibres during the tensile failure, and of the energy $E_m^{(de)}$ absorbed by the matrix during the delamination process, i.e.:

$$E_s = E_f^{(te)}\ V_f + E_m^{(de)}\,(1 - V_f) \tag{2}$$

The fitting procedure of the experimental values of E_s (see Tab.5) by using the straight line represented by Eq.2 (see Fig.9), permits to compute immediately the unknown values of the specific energy $E_f^{(te)}$ and $E_m^{(de)}$; it provides:

$$E_f^{(te)} = 42.29 \text{ J}; \qquad E_m^{(de)} = 3.07 \text{ J}$$

From such values it is possible to observe how under longitudinal tensile loading the impact strength $E_f^{(te)}$ of the fibers is about 4 times higher than the above determined strength $E_f^{(sp)}$ of the same fibres under transversal tensile loading (splitting); also, as it is expected, the matrix impact strength $E_m^{(de)}$ associated to the interlaminar delamination is higher (about +72%) than the strength $E_m^{(te)}$ of the same matrix associated to tensile loading (it is well known, in fact, that under shear loading the thermosetting resins exhibits more plasticity than under tensile loading).

5.3 QI laminates

The impact tests performed the on the quasi-isotropic biocomposites laminates have shown that the perforation of such laminates occurs for the same impact energies before detected for the CP laminates (20 J, 25 J and 30 J for V_f =35%, 50% and 70% respectively), as it is shown in Figs.6e and 6f concerning the two extreme V_f =35% and 70% cases. Similar are also the main damaging processes observed: fibre failure by longitudinal tensile and matrix collapse by shear associated with interlaminar delamination. Also in this case, the damaged zone of the front surface has the circular shape of the impactor, whereas the damaged zone of the back surface appears characterized by irregular shape with dimension superior to the impactor, with evident delamination phenomena.

Also, the analysis of the characteristic impact curves and of the numerical values reported in Tab.5, shows that, similarly to CP laminates, both F_i^{FID} and F_i^{MAX} increase appreciably with V_f ; in detail, passing from V_f =35% to V_f =70% F_i^{FID} increases of about 180%, whereas F_i^{MAX} redoubles as V_f. Moreover, the absorbed elastic energy increases significantly (+230%) by passing from 3.2 J to 10.8 J, whereas the impact strength increases from 18.9 J to 29.8 J (about +60%), with increments that are also in this case almost directly proportional to V_f. From the similar results in terms of total absorbed energy, it possible to state that the QI biocomposites laminates have in practice the same impact strength of the CP biocomposite laminates. Consequently, Eq.2 and the values of $E_f^{(te)}$ and $E_m^{(de)}$ above determined for the CP laminates can be applied also to the QI laminates.

Although wider delamination phenomena are observed in the CP laminates, the overall contribution of the delamination processes to the impact strength of the biocomposite is in practice the same due to the reduced specific absorbed energy compared to the QI case that is characterized by higher specific energy, due to higher critical stress delamination values, as confirmed also by the higher values of F_i^{FID} shown in Tab.5 (values included between 1850 N and 3350 N for QI, between 1175 N and 2825 N for CP). It is possible therefore to state that although the impact strength of the CP and QI laminates is comparable, the QI laminates are slightly more suitable for impact loading, because the impact damage of the CP laminate starts for lower loads or, for a fixed impact energy, the QI laminates exhibit more limited damaged surfaces.

5.4 MAT laminates

The experimental evidence has shown that the complete penetration (perforation) of the MAT biocomposites with V_f =15% and 35% is given by an impact energy E_i =10 J, whereas for V_f =30% it needs an impacting energy E_i =15 J. In other words, it is seen how the impact strength increases with fiber volume fraction but only up to V_f =30%, whereas it decreases for V_f > 30%. This particular non monotonic behaviour is similar to what has already been observed for these biocomposites in the preliminary tensile tests: under static conditions the tensile strength of such MAT biocomposites has a non-monotonic trend, and the maximum strength corresponds to V_f =30% (see Tab.4). This behaviour is due to the high moulding pressure needed to obtain MAT biocomposites with V_f > 30%, that determines the direct contact of the fibres (without interposed matrix) which corresponds to the formation of fibre/fibre interface cracks, with consequent significant mechanical strength reduction due to premature damage mechanisms relating to the propagation of such cracks.

For the examined MAT biocomposites the highest impact strength corresponds to the laminate having V_f = 30% that exhibits a total energy absorption of 13.9 J (see Tab.5).

In terms of damage processes (see Figs.6g and 6h), similarly to what has already been observed in the static case, the experimental analysis shows that also under impact loading the local damage of the MAT biocomposites involves a mixed process consisting of 4 different phenomena: (a) tensile failure of the longitudinal fibers (locally aligned with the maximum tensile stress), (b) matrix collapse under tensile stress, (c) secondary pull-out (concerning the fibers not-aligned with the local maxim tensile stress) and (c) splitting phenomena of the transverse fibres (fibres parallel with the local surface fracture).

Taking into account such particular damage mechanisms, it is possible to state that, like it has been proposed in [51] concerning the tensile strength of short fiber biocomposites, the impact strength of the MAT biocomposites having $V_f \leq 30\%$ can be accurately estimated by considering a quasi-isotropic model [0/±60]. In detail, by considering that in such a model the formation of a surface fracture in a generic direction corresponds in practice to:

1) the tensile failure of the fibres orthogonal to the fracture surface (1/3 of the total fibers);
2) the partial pull-out of about 1/2 of the fibers orthogonal to the fracture surface (1/6 of the total fibers);
3) the splitting failure of the fibers not aligned with the fracture surface (2/3 of the total fibres);
4) the tensile failure of the matrix;

by using the specific energy values $E_f^{(sp)}$, $E_f^{(te)}$, $E_m^{(te)}$ above already determined for the same damage mechanisms observed in unidirectional laminates (fibre failure by splitting and matrix failure by

tensile) and angle-ply laminates (fibre failure by longitudinal tensile), and by indicating with $E_f^{(pu)}$ the specific energy associated to the pull-out, the following energy-balance equation can be written:

$$E_s = \frac{1}{3}E_f^{(te)} V_f + \frac{1}{6}E_f^{(pu)} V_f + \frac{2}{3}E_f^{(sp)} V_f + E_m^{(te)}(1 - V_f) \quad (3)$$

The unknown value of $E_f^{(pu)}$ can be determined by fitting the experimental values of E_s reported in Tab.5 for V_f = 15% and 30% with the straight line represented by Eq.3; it provides:

$$E_f^{(pu)} = 97.26 \text{ J}$$

As it has been noted by other authors in [108,109], the energy $E_f^{(pu)}$ absorbed by fiber pull-out is higher than the energy $E_f^{(te)}$= 42.29 J absorbed by the same fibre for longitudinal tensile failure.

Fig.10 shows the comparison between the impact strength predicted by the proposed quasi-isotropic model (Eq.3) and the experimental data; it is seen a good agreement for $V_f \leq$ 30%. Therefore, such a model can be used advantageously at the design stage to determine the impact strength of good quality MAT biocomposites reinforced by sisal fibers.

5.5 Brief comparative analysis of the results

The comparison of the results reported in Tab.5 and represented graphically in the following Fig.11a in terms of impact strength for the various biocomposites examined, shows synthetically that the UD biocomposites laminates exhibits the lower impact performances that reach the maximum value of E_s ≈ 10 J for V_f =70%. Relatively better performance is exhibited by the MAT laminates that reach the maximum value of E_s =13.9 J for the optimal value of V_f =30%. However, such impact performances are appreciably inferior to those exhibited by the angle-ply (CP and QI) laminates, that reach the maximum values of E_s ≈ 30 J for V_f =70%.

In terms of first impact damage force F_i^{FID} instead, the UD laminates exhibits performance always better than the MAT laminates, and also better than the CP laminates for $V_f \leq$ 50% (see Fig.11b). However, for any V_f value the higher values of F_i^{FID} are exhibited always by the QI lay-up, that is therefore the best lay-up to be used for the manufacturing of light and green components subjected to impact loading, because it exhibits both the maxim impact strength and the maximum first impact damage force.

5.6 Internal damage investigations by computed tomography

Due to the complexity of the damage mechanisms related to the impact tests, the direct visual inspection of the impacted specimens leads to an underestimation of the actual damage; also, the damage processes interesting the internal laminae of the UD, CP and QI laminates (e.g. internal

delaminations etc.) are difficult to observe. In order to obtain a more accurate and complete analysis of the impact damage, a three-dimensional reconstruction of the specimens subjected to mechanical failure have been to obtained through a 3D Computed Tomography System (Y.CT Vario International GmbH, Hamburg, Germany), by using a source voltage of 190 kV and 1 mA. In detail, the 3D profile generation has been carried out by using 1440 projections with rotation steps of 0.5°. The reconstruction and the results analysis have been carried out by means of software VGStudio Max 2.0 by Volume Graphics GmbH.

As an example, Fig.12 shows two tomographic images of one of the UD specimens having V_f=35%, that confirms the primary failure mechanism observed visually during the test, consisting on the formation and propagation of a through thickness cracks parallel to the direction of the fibres (Fig.12a); also, limited delamination phenomena concentrated in the impact zone are also observed (Fig.12b). Qualitatively similar results have been observed for the other V_f values considered.

Fig.13 shows two tomographic images of a CP specimen with V_f=35% after the impact test carried out by using an impact energy E_i =10 J (less than the impact strength of 16.1 J). Qualitatively similar results have been observed for the other V_f and E_i values considered. In detail, the two damage mechanism already observed by visual inspection, i.e. the interlaminar delamination (Fig.13a) and the fibre failure by tensile load (Fig.13b), both related to the local bending produced by the impact loading, are clearly confirmed.

Lastly, Fig.14 shows two tomographic images of one of the QI specimens having V_f=35%, subjected to an impact energy of 10 J (less than the impact strength of 18.9 J). From such figure it is possible to state that there is no substantial difference with the CP specimens, i.e. also in this case the damage process involves interlaminar delamination phenomena (Fig.14a) and fibre failure by longitudinal tensile (Fig.14b), although, as it has been noted above by considering the higher values of the first impact damage force, the delamination phenomena appear significantly less extensive with respect to those observed for the CP laminates (see Fig.13).

6. COMPARISON WITH OTHER LITERATURE RESULTS

In order to compare the impact performance of the biocomposites analyzed with those of other biocomposites and composites reinforced by synthetic fibers, the main results available in literature for such materials, included binary and ternary composites and biocomposites, have been reported in Tab.6.

In detail, for each material considered Tab.6 shows the relative lay-up, density (ρ), thickness (t_s) of the specimens used for the impact tests, fiber volume fraction (V_f), impact energy (E_i) and the impact strength (E_s). In order to take into account the different thickness of the specimens used by the various authors for the impact tests, as well as of the different specific weight of the materials, the comparison is performed by considering the so called specific impact strength E_s^* obtained by dividing the impact

strength E_s to the specimen thickness t_s and to the material density ρ (see the penultimate column of Tab.6). For a more immediate comparison such values are also reported in the bar graph of Fig.15.

From the analysis of such data it is first observed how the specific impact strength of the materials reported in literature, varies in a wide range, from the minimum value of 1690 J mm^2 g^{-1} of a CP juta/glass-polyester hybrid biocomposite, up to the maximum value of 7290 J mm^2 g^{-1} of a QI kevlar/carbon-epoxy hybrid composite.

In particular, from Tab.6 and Fig.15 it is seen how the biocomposites reinforced by sisal fibers considered in the present work, exhibit a specific impact strength ranging from 1950 J mm^2 g^{-1} for the UD laminate with V_f =70%, to 3150 J mm^2 g^{-1} for the MAT laminate with V_f =30%, to about 6300 J mm^2 g^{-1} for the angle-ply (CP and QI) laminates with V_f =70%.

The biocomposites reinforced by other natural fibers (flax, hemp, jute), commonly manufactured by CP woven fabrics with V_f = 20%÷60%, exhibit similar specific impact strengths included between 1890 J mm^2 g^{-1} (hemp/epoxy) and 5840 J mm^2 g^{-1} (hemp/PLA).

Concerning the traditional composites reinforced by synthetic fibers, the GFRP shows a relatively high specific impact strength, passing from 5420 to 6550 J mm^2 g^{-1} by moving from the UD laminates to the more resistant CP laminates. Significantly lower values are exhibited by the CFRP composites, varying between 1910 J mm^2 g^{-1} (V_f≈30%) and 4120 J mm^2 g^{-1} (V_f≈60%). Values higher than GFRP are instead shown by cross-ply KFRP composites with V_f=60% (7120 J mm^2 g^{-1}).

Also, the composites recently proposed in literature reinforced by basalt fibers, usually realized by woven fabrics with V_f = 30%÷50%, are characterized by specific impact strength falling in the range 3190÷6420 J mm^2 g^{-1}.

However, the best impact performance corresponds to the QI hybrid composites reinforced by synthetic fibers, whose E_S^* value varies in the range 5450÷7290 J mm^2 g^{-1}.

Relatively lower values are instead shown by the hybrid composites reinforced by natural and synthetic fibers whose E_S^* value varies in a wide range included between 1690 J mm^2 g^{-1} (jute/glass-polyester) and 6050 J mm^2 g^{-1}(flax/basalt/hemp-epoxy).

Synthetically, it is possible to state that the best impact performance are exhibited from the angle-ply (CP and QI) biocomposites reinforced by an sisal with volume fraction of 70%; their specific impact strenght E_S^* ≈ 6300 J mm^2 g^{-1} is in practice:

1) light higher than that (E_S^* ≈ 5840 J mm^2 g^{-1}) of the best biocomposite reported in literature (CP laminate reinforced by hemp fibers);
2) comparable with that of the best GFRP (E_S^* ≈6550 J mm^2 g^{-1}), as well as with that of the composites reinforced by basalt fibers (E_S^*≈6420 J mm^2 g^{-1}), and of the ternary hybrid kevlar-carbon-glass composites (E_S^* ≈6190 J mm^2 g^{-1});
3) appreciably higher (+15÷50%) than that of the best CFRP (E_S^* ≈4120 J mm^2 g^{-1}) and of the hybrid carbon-glass composites (E_S^* ≈5450 J mm^2 g^{-1});

4) slight lower (-14% circa) than that of the performing binary hybrid kevlar-glass composites ($E^*_S \approx 7200$ J mm^2 g^{-1}) and kevlar-carbon composites ($E^*_S \approx 7300$ J mm^2 g^{-1}).

Such results confirm widely the worthy impact performance expected by the biocomposite reinforced by sisal fiber; it is fully corroborated that the sub-fibrillar structure of the sisal fiber leads to a good impact strength, higher than that of other biocomposites reported in literature, and comparable with that of the more polluting, expensive and weighty composites reinforced by synthetic fibers. Renewability, cost and weight are important parameters that have to be properly highlighted in the comparison between the examined biocomposites and the synthetic composites: thanks to the low cost (about 0.3 €/kg in the international market) and low weight (about 1450 kg/m^3, lower than that any synthetic fiber) of the sisal fiber, the analyzed biocomposites have in fact cost and weight significantly lower than that of the traditional synthetic composites. Therefore, it is possible to state that, as expected by the scientific community, such biocomposites can substitute the synthetic composites in the practical applications characterized by high impact loading (bumpers, helmets, protection systems against impact etc.), with a contemporary advantageous reduction not only of the environmental pollution but, very important, also of the costs and of the weight (that can lead to further advantageous reduction of the consumption if the component is used in the automotive field).

7. CONCLUSIONS

Through a systematic campaign of experimental tests the response to the low velocity impact loading of biocomposite laminates reinforced by sisal fibers, by varying the main influence parameters as the fiber distribution (unidirectional, random), the fiber volume fraction V_f and the lay-up (unidirectional, cross-ply, quasi-isotropic and MAT), has been analyzed.

In particular, such an experimental analysis has shown that the more performing lay-ups (specific impact strength E^*_S= 6300 J mm^2 g^{-1}) are the angle-ply one (cross-ply and quasi-isotropic) whose damage under impact loading involves advantageously the longitudinal failure of all the fibers for tensile loading, damage mechanism that is characterized by an high value of the impact energy absorption (42.29 J).

Much lower are instead the performance of the unidirectional laminates (E^*_S= 1950 J mm^2 g^{-1}) because the impact failure occurs always by transversal tensile failure that involves the transversal fiber splitting mixed to the matrix tensile failure, which correspond low values of the impact energy absorption (9.84 J and 1.79 J respectively).

Although higher than that of the unidirectional laminates, the impact strength of the MAT laminates is also relatively modest (E^*_S= 3150 J mm^2 g^{-1}), due to the limited fiber volume fraction that can be used in this particular lay-up (maximum value of 30%) to obtain good quality laminates. The improvement of the impact strength with respect to the unidirectional laminates is essentially due to the particular damage mechanisms involved, as the longitudinal tensile failure of the fibers aligned with the maxim

stress and, above all, the partial pull-out, characterized by the highest value of the impact energy absorption (97.26 J).

The accurate analysis of the experimental results in terms of impact strength, has permitted the implementation of simple models that have allowed first the evaluation of the impact energy absorption associated to the various damage mechanisms observed (longitudinal tensile failure of the fibers, fiber splitting, interlaminar delamination and pull-out), and can be used at the design stage for reliable prediction of the impact strength of the various laminates by varying the fiber volume fraction. The peculiar damage mechanisms observed by visual inspection have been widely confirmed by an accurate internal 3D computed tomography investigation.

Finally, the comparison between the specific impact strength of the examined biocomposites with that of other biocomposites and composites reported in literature, has allowed to corroborate that, as it was expected, the biocomposites reinforced by sisal fibers exhibit a high impact strength, that is higher (from +10 to +50%) than that of the biocomposites reinforced by other natural fibers (jute, hemp, flax), as well as of the composites reinforced by carbon fibers ternary kevlar-carbon-glass systems. Also, their impact strength is only slight lower than that of much more expensive, polluting and weighty hybrid kevlar-glass and kevlar-carbon composites.

Taking into account the fully renewability, the low cost and the low weight of the sisal fiber it is therefore possible to state that the biocomposites reinforced by sisal fibers can be used in various industrial fields to substitute the synthetic composites for the manufacturing of protection systems against impact (bumpers, helmets etc.), obtaining in such a way not only a reduction of the environmental pollution but also a contemporary advantageously reduction of costs and weight.

Further studies on the examined biocomposites will focused to the expected improving of the impact strength, associated with the substitution of the unidirectional stitched fabrics with woven fabrics, properly implemented for such a scope.

Data availability statement

The raw/processed data required to reproduce these findings cannot be shared at this time as the data also forms part of an ongoing study.

References

[1] Koronis G, Silva A, Fontul M. Green composites: A review of adequate materials for automotive applications. Compos Part B Eng 2013;44:120–7. https://doi.org/10.1016/j.compositesb.2012.07.004.

[2] Nabi Saheb D, Jog JP. Natural fiber polymer composites: A review. Adv Polym Technol 1999;18:351–63. https://doi.org/10.1002/(SICI)1098-2329(199924)18:4<351::AID-ADV6>3.0.CO;2-X.

[3] Ku H, Wang H, Pattarachaiyakoop N, Trada M. A review on the tensile properties of natural fiber reinforced polymer composites. Compos Part B Eng 2011;42:856–73. https://doi.org/10.1016/j.compositesb.2011.01.010.

[4] Jagadeesh D, Kanny K, Prashantha K. A Review on Research and Development of Green Composites From Plant Protein-Based Polymers. Polym Compos 2016;37:915–24. https://doi.org/10.1002/pc.

[5] Bharath KN, Basavarajappa S. Applications of biocomposite materials based on natural fibers from renewable resources: A review. Sci Eng Compos Mater 2016;23:123–33. https://doi.org/10.1515/secm-2014-0088.
[6] Ramesh M, Palanikumar K, Reddy KH. Plant fibre based bio-composites: Sustainable and renewable green materials. Renew Sustain Energy Rev 2017;79:558–84. https://doi.org/10.1016/j.rser.2017.05.094.
[7] Shekar HSS, Ramachandra M. Green Composites: A Review. Mater Today Proc 2018;5:2518–26. https://doi.org/10.1016/j.matpr.2017.11.034.
[8] Benzait Z, Trabzon L. A review of recent research on materials used in polymer–matrix composites for body armor application. J Compos Mater 2018;52:3241–63. https://doi.org/10.1177/0021998318764002.
[9] Sanjay MR, Madhu P, Jawaid M, Senthamaraikannan P, Senthil S, Pradeep S. Characterization and properties of natural fiber polymer composites: A comprehensive review. J Clean Prod 2018;172:566–81. https://doi.org/10.1016/j.jclepro.2017.10.101.
[10] Khan T, Hameed Sultan MT Bin, Ariffin AH. The challenges of natural fiber in manufacturing, material selection, and technology application: A review. J Reinf Plast Compos 2018;37:770–9. https://doi.org/10.1177/0731684418756762.
[11] Mohammed L, Ansari MNM, Pua G, Jawaid M, Islam MS. A Review on Natural Fiber Reinforced Polymer Composite and Its Applications. Int J Polym Sci 2015;2015. https://doi.org/10.1155/2015/243947.
[12] Nunna S, Chandra PR, Shrivastava S, Jalan AK. A review on mechanical behavior of natural fiber based hybrid composites. J Reinf Plast Compos 2012;31:759–69. https://doi.org/10.1177/0731684412444325.
[13] Faruk O, Bledzki AK, Fink HP, Sain M. Biocomposites reinforced with natural fibers: 2000-2010. Prog Polym Sci 2012;37:1552–96. https://doi.org/10.1016/j.progpolymsci.2012.04.003.
[14] Bendigeri C, Jwalesh HN. Review on Fatigue behaviour of Polymeric Biomaterials with Natural Fibers 2016:3–6.
[15] Mortazavian S, Fatemi A. Fatigue of short fiber thermoplastic composites: A review of recent experimental results and analysis. Int J Fatigue 2017;102:171–83. https://doi.org/10.1016/j.ijfatigue.2017.01.037.
[16] Yan L, Kasal B, Huang L. A review of recent research on the use of cellulosic fibres, their fibre fabric reinforced cementitious, geo-polymer and polymer composites in civil engineering. Compos Part B Eng 2016;92:94–132. https://doi.org/10.1016/j.compositesb.2016.02.002.
[17] Pickering KL, Efendy MGA, Le TM. A review of recent developments in natural fibre composites and their mechanical performance. Compos Part A Appl Sci Manuf 2016;83:98–112. https://doi.org/10.1016/j.compositesa.2015.08.038.
[18] Dicker MPM, Duckworth PF, Baker AB, Francois G, Hazzard MK, Weaver PM. Green composites: A review of material attributes and complementary applications. Compos Part A Appl Sci Manuf 2014;56:280–9. https://doi.org/10.1016/j.compositesa.2013.10.014.
[19] Ahmad F, Choi HS, Park MK. A review: Natural fiber composites selection in view of mechanical, light weight, and economic properties. Macromol Mater Eng 2015;300:10–24. https://doi.org/10.1002/mame.201400089.
[20] Jayanth D, Kumar PS, Nayak GC, Kumar JS, Pal SK, Rajasekar R. A Review on Biodegradable Polymeric Materials Striving Towards the Attainment of Green Environment. J Polym Environ 2018;26:838–65. https://doi.org/10.1007/s10924-017-0985-6.
[21] Mohanty AK, Manjusri M, Lawrence DT. Natural Fibers , Biopolymers , and Biocomposites. CRC Press. 2005.
[22] Shah DU. Natural fibre composites: Comprehensive Ashby-type materials selection charts. Mater Des 2014;62:21–31. https://doi.org/10.1016/j.matdes.2014.05.002.
[23] Gomes A, Matsuo T, Goda K, Ohgi J. Development and effect of alkali treatment on tensile properties of curaua fiber green composites. Compos Part A Appl Sci Manuf 2007;38:1811–20. https://doi.org/10.1016/j.compositesa.2007.04.010.
[24] Preet Singh JI, Dhawan V, Singh S, Jangid K. Study of Effect of Surface Treatment on Mechanical Properties of Natural Fiber Reinforced Composites. Mater Today Proc 2017;4:2793–9. https://doi.org/10.1016/j.matpr.2017.02.158.
[25] Kaewkuk S, Sutapun W, Jarukumjorn K. Effects of interfacial modification and fiber content on physical

properties of sisal fiber/polypropylene composites. Compos Part B Eng 2013;45:544–9. https://doi.org/10.1016/j.compositesb.2012.07.036.
[26] Bisanda ETN, Ansell MP. The effect of silane treatment on the mechanical and physical properties of sisal-epoxy composites. Compos Sci Technol 1991;41:165–78. https://doi.org/10.1016/0266-3538(91)90026-L.
[27] Joseph K, Thomas S, Pavithran C. Effect of chemical treatment on the tensile properties of short sisal fibre-reinforced polyethylene composites. Polymer (Guildf) 1996;37:5139–49. https://doi.org/10.1016/0032-3861(96)00144-9.
[28] Singh B, Gupta M, Verma A. Influence of Fiber Surface Treatment on the Properties of Sisal-Polyester Composites. Polym Compos 1996;17:910–8. https://doi.org/https://doi.org/10.1002/pc.10684.
[29] Mylsamy K, Rajendran I. Influence of alkali treatment and fibre length on mechanical properties of short Agave fibre reinforced epoxy composites. Mater Des 2011;32:4629–40. https://doi.org/10.1016/j.matdes.2011.04.029.
[30] Kim JT, Netravali AN. Mercerization of sisal fibers: Effect of tension on mechanical properties of sisal fiber and fiber-reinforced composites. Compos Part A Appl Sci Manuf 2010;41:1245–52. https://doi.org/10.1016/j.compositesa.2010.05.007.
[31] Sood M, Dwivedi G. Effect of fiber treatment on flexural properties of natural fiber reinforced composites: A review. Egypt J Pet 2018;27:775–83. https://doi.org/10.1016/j.ejpe.2017.11.005.
[32] Ramzy A, Beermann D, Steuernagel L, Meiners D, Ziegmann G. Developing a new generation of sisal composite fibres for use in industrial applications. Compos Part B Eng 2014;66:287–98. https://doi.org/10.1016/j.compositesb.2014.05.016.
[33] Li Y, Ma H, Shen Y, Li Q, Zheng Z. Effects of resin inside fiber lumen on the mechanical properties of sisal fiber reinforced composites. Compos Sci Technol 2015;108:32–40. https://doi.org/10.1016/j.compscitech.2015.01.003.
[34] Li Y, Mai Y, Ye L. Sisal fibre and its composites : a review of recent developments IM PA US AS DO ME US EX ON AS. Compos Sci Technol 2000;60:2037–55.
[35] Sreekumar PA, Joseph K, Unnikrishnan G, Thomas S. A comparative study on mechanical properties of sisal-leaf fibre-reinforced polyester composites prepared by resin transfer and compression moulding techniques. Compos Sci Technol 2007;67:453–61. https://doi.org/10.1016/j.compscitech.2006.08.025.
[36] Cirello A, Zuccarello B. On the effects of a crack propagating toward the interface of a bimaterial system. Eng Fract Mech 2006;73:1264–77. https://doi.org/10.1016/j.engfracmech.2005.12.003.
[37] Murherjee P, Satyananrayana K. Structure and properties of some vegetable fibres, part. 1 Sisal Fibres. J Mater Sci 1986;19:3925–6.
[38] Bezazi A, Belaadi A, Bourchak M, Scarpa F, Boba K. Novel extraction techniques, chemical and mechanical characterisation of Agave americana L. natural fibres. Compos Part B Eng 2014;66:194–203. https://doi.org/10.1016/j.compositesb.2014.05.014.
[39] Chand N, Hashmi SAR. Mechanical properties of sisal fibre at elevated temperatures. J Mater Sci 1993;28:6676–82. https://doi.org/10.1007/BF00356422.
[40] Chand N, Verma S, Khazanchi AC. SEM and strength characteristics of acetylated sisal fibre. J Mater Sci Lett 1989;8:1307–9. https://doi.org/10.1007/BF00721503.
[41] Silva F de A, Chawla N, Filho RD de T. Tensile behavior of high performance natural (sisal) fibers. Compos Sci Technol 2008;68:3438–43. https://doi.org/10.1016/j.compscitech.2008.10.001.
[42] Thomason JL, Carruthers J, Kelly J, Johnson G. Fibre cross-section determination and variability in sisal and flax and its effects on fibre performance characterisation. Compos Sci Technol 2011;71:1008–15. https://doi.org/10.1016/j.compscitech.2011.03.007.
[43] Belaadi A, Bezazi A, Bourchak M, Scarpa F, Zhu C. Thermochemical and statistical mechanical properties of natural sisal fibres. Compos Part B Eng 2014;67:481–9. https://doi.org/10.1016/j.compositesb.2014.07.029.
[44] Milanese AC, Cioffi MOH, Voorwald HJC. Thermal and mechanical behaviour of sisal/phenolic composites. Compos Part B Eng 2012;43:2843–50. https://doi.org/10.1016/j.compositesb.2012.04.048.
[45] Towo AN, Ansell MP. Fatigue evaluation and dynamic mechanical thermal analysis of sisal fibre-thermosetting resin composites. Compos Sci Technol 2008;68:925–32. https://doi.org/10.1016/j.compscitech.2007.08.022.

[46] Belaadi A, Bezazi A, Maache M, Scarpa F. Fatigue in sisal fiber reinforced polyester composites: Hysteresis and energy dissipation. Procedia Eng 2014;74:325–8. https://doi.org/10.1016/j.proeng.2014.06.272.
[47] Zuccarello B. Static and dynamic mechanical properties of eco-friendly polymer composites. Sustain. Polym. Compos. Nanocomposites Springer Nat., 2019, p. 259–92. https://doi.org/10.1007/978-3-030-05399-4_9.
[48] Zuccarello B, Zingales M. Toward high performance renewable agave reinforced biocomposites: Optimization of fiber performance and fiber-matrix adhesion analysis. Compos Part B Eng 2017;122:109–20. https://doi.org/10.1016/j.compositesb.2017.04.011.
[49] Zuccarello B, Scaffaro R. Experimental analysis and micromechanical models of high performance renewable agave reinforced biocomposites. Compos Part B Eng 2017;119:141–52. https://doi.org/10.1016/j.compositesb.2017.03.056.
[50] Zuccarello B, Marannano G, Mancino A. Optimal manufacturing and mechanical characterization of high performance biocomposites reinforced by sisal fibers. Compos Struct 2018;194:575–83. https://doi.org/10.1016/j.compstruct.2018.04.007.
[51] Zuccarello B, Marannano G. Random short sisal fiber biocomposites: Optimal manufacturing process and reliable theoretical models. Mater Des 2018;149:87–100. https://doi.org/10.1016/j.matdes.2018.03.070.
[52] Pantano A, Zuccarello B. Numerical model for the characterization of biocomposites reinforced by sisal fibres. Procedia Struct Integr 2018;8:517–25. https://doi.org/10.1016/j.prostr.2017.12.051.
[53] Mancinoa A, Marannano G, Zuccarello B. Implementation of eco-sustainable biocomposite materials reinforced by optimized agave fibers. Procedia Struct Integr 2018;8:526–38. https://doi.org/10.1016/j.prostr.2017.12.052.
[54] Incorvaia D, Zingales M, Zuccarello B. Analisi sperimentale del comportamento meccanico di bio-compositi rinforzati con fibre di agave. 44° ASIAS Natl. Conf., Messina: 2015.
[55] Incorvaia D, Scaffaro R, Zuccarello B. Analisi del comportamento meccanico di sandwich eco-compatibili rinforzati con fibre naturali. 44° ASIAS Natl. Conf., Messina: 2015.
[56] Zuccarello B, Scaffaro R, Zingales M. Progettazione efficiente di biocompositi rinforzati con fibre di agave. 45° ASIAS Natl. Conf., Trieste: 2016.
[57] Zuccarello B, Mancino A, Sarno M, Zingales M. Analisi del comportamento meccanico di diverse varietà di Fibre di agave e dei relativi biocompositi ecosostenibili. 46° ASIAS Natl. Conf., Pisa: 2017.
[58] Zuccarello B, Marannano G, Bongiorno F. Resistenza statica e a fatica di nuovi laminati biocompositi rinforzati con fibre di agave. 47° ASIAS Natl. Conf., Reggio Calabria: 2018.
[59] Militello C, Epasto G, Zuccarello B. Valutazione del comportamento all' impatto di biocompositi rinforzati con fibre di agave. 48° ASIAS Natl. Conf., Assisi: 2019.
[60] Bongiorno F, Militello C, Zuccarello B. Resistenza alla frattura translaminare di biocompositi rinforzati con fibre di agave. 48° ASIAS Natl. Conf., Assisi: 2019.
[61] Petrucci R, Santulli C, Puglia D, Nisini E, Sarasini F, Tirillò J, et al. Impact and post-impact damage characterisation of hybrid composite laminates based on basalt fibres in combination with flax, hemp and glass fibres manufactured by vacuum infusion. Compos Part B Eng 2015;69:507–15. https://doi.org/10.1016/j.compositesb.2014.10.031.
[62] Liang S, Guillaumat L, Gning PB. Impact behaviour of flax/epoxy composite plates. Int J Impact Eng 2015;80:56–64. https://doi.org/10.1016/j.ijimpeng.2015.01.006.
[63] Wang W, Chouw N, Jayaraman K. Effect of thickness on the impact resistance of flax fibre-reinforced polymer. J Reinf Plast Compos 2016;35:1277–89. https://doi.org/10.1177/0731684416648780.
[64] Al-Hajaj Z, Sy BL, Bougherara H, Zdero R. Impact properties of a new hybrid composite material made from woven carbon fibres plus flax fibres in an epoxy matrix. Compos Struct 2019;208:346–56. https://doi.org/10.1016/j.compstruct.2018.10.033.
[65] Sarasini F, Tirillò J, Ferrante L, Valente M, Valente T, Lampani L, et al. Drop-weight impact behaviour of woven hybrid basalt-carbon/epoxy composites. Compos Part B Eng 2014;59:204–20. https://doi.org/10.1016/j.compositesb.2013.12.006.
[66] Sarasini F, Tirillò J, D'Altilia S, Valente T, Santulli C, Touchard F, et al. Damage tolerance of carbon/flax hybrid composites subjected to low velocity impact. Compos Part B Eng 2016;91:144–53.

https://doi.org/10.1016/j.compositesb.2016.01.050.
[67] Živković I, Fragassa C, Pavlović A, Brugo T. Influence of moisture absorption on the impact properties of flax, basalt and hybrid flax/basalt fiber reinforced green composites. Compos Part B Eng 2017;111:148–64. https://doi.org/10.1016/j.compositesb.2016.12.018.
[68] Ravandi M, Teo WS, Tran LQN, Yong MS, Tay TE. Low velocity impact performance of stitched flax/epoxy composite laminates. Compos Part B Eng 2017;117:89–100. https://doi.org/10.1016/j.compositesb.2017.02.003.
[69] Nisini E, Santulli C, Liverani A. Mechanical and impact characterization of hybrid composite laminates with carbon, basalt and flax fibres. Compos Part B Eng 2017;127:92–9. https://doi.org/10.1016/j.compositesb.2016.06.071.
[70] Fragassa C, Pavlovic A, Santulli C. Mechanical and impact characterisation of flax and basalt fibre vinylester composites and their hybrids. Compos Part B Eng 2018;137:247–59. https://doi.org/10.1016/j.compositesb.2017.01.004.
[71] Ricciardi MR, Papa I, Lopresto V, Langella A, Antonucci V. Effect of hybridization on the impact properties of flax/basalt epoxy composites: Influence of the stacking sequence. Compos Struct 2019;214:476–85. https://doi.org/10.1016/j.compstruct.2019.01.087.
[72] Caprino G, Carrino L, Durante M, Langella A, Lopresto V. Low impact behaviour of hemp fibre reinforced epoxy composites. Compos Struct 2015;133:892–901. https://doi.org/10.1016/j.compstruct.2015.08.029.
[73] Feldmann M, Verheyen F. Impact behavior of continuous biaxial reinforced composites based on bio-polyamides and man-made cellulose fibres. Int Polym Process 2016;31:198–206. https://doi.org/10.3139/217.3142.
[74] Dhakal HN, Ismail SO, Jiang C, Zhang Z, Sweatman T. Influence of barely visible impact damage on post-impact residual flexural properties of hybrid Fibri Rock – Aero Eco-composites. Mater Lett 2018;233:233–7. https://doi.org/10.1016/j.matlet.2018.09.036.
[75] Dhakal H, Bourmaud A, Berzin F, Almansour F, Zhang Z, Shah DU, et al. Mechanical properties of leaf sheath date palm fibre waste biomass reinforced polycaprolactone (PCL) biocomposites. Ind Crops Prod 2018;126:394–402. https://doi.org/10.1016/j.indcrop.2018.10.044.
[76] Dhakal HN, Zhang ZY, Richardson MOW, Errajhi OAZ. The low velocity impact response of non-woven hemp fibre reinforced unsaturated polyester composites. Compos Struct 2007;81:559–67. https://doi.org/10.1016/j.compstruct.2006.10.003.
[77] Ismail MF, Sultan MTH, Hamdan A, Shah AUM. A study on the low velocity impact response of hybrid Kenaf-Kevlar composite laminates through drop test rig technique. BioResources 2018;13:3045–60. https://doi.org/10.15376/biores.13.2.3045-3060.
[78] Puech L, Ramakrishnan KR, Le Moigne N, Corn S, Slangen PR, Duc A Le, et al. Investigating the impact behaviour of short hemp fibres reinforced polypropylene biocomposites through high speed imaging and finite element modelling. Compos Part A Appl Sci Manuf 2018;109:428–39. https://doi.org/10.1016/j.compositesa.2018.03.013.
[79] Nor AFM, Sultan MTH, Jawaid M, Azmi AMR, Shah AUM. Analysing impact properties of CNT filled bamboo/glass hybrid nanocomposites through drop-weight impact testing, UWPI and compression-after-impact behaviour. Compos Part B Eng 2019;168:166–74. https://doi.org/10.1016/j.compositesb.2018.12.061.
[80] Ahmed KS, Vijayarangan S, Kumar A. Low velocity impact damage characterization of woven jute-glass fabric reinforced isothalic polyester hybrid composites. J Reinf Plast Compos 2007;26:959–76. https://doi.org/10.1177/0731684407079414.
[81] Al-Maharma AY, Sendur P. Review of the main factors controlling the fracture toughness and impact strength properties of natural composites. Mater Res Express 2019;6. https://doi.org/10.1088/2053-1591/aaec28.
[82] Thanomsilp C, Hogg PJ. Penetration impact resistance of hybrid composites based on commingled yarn fabrics. Compos Sci Technol 2003;63:467–82. https://doi.org/10.1016/S0266-3538(02)00233-6.
[83] Dear JP, Brown SA. Impact damage processes in reinforced polymeric materials. Compos Part A Appl Sci Manuf 2003;34:411–20. https://doi.org/10.1016/S1359-835X(03)00082-4.
[84] Arikan V, Sayman O. Comparative study on repeated impact response of E-glass fiber reinforced

polypropylene & epoxy matrix composites. Compos Part B Eng 2015;83:1–6. https://doi.org/10.1016/j.compositesb.2015.08.051.
[85] Yan R, Wang R, Lou CW, Lin JH. Low-velocity impact and static behaviors of high-resilience thermal-bonding inter/intra-ply hybrid composites. Compos Part B Eng 2015;69:58–68. https://doi.org/10.1016/j.compositesb.2014.09.021.
[86] Lopresto V, Melito V, Leone C, Caprino G. Effect of stitches on the impact behaviour of graphite/epoxy composites. Compos Sci Technol 2006;66:206–14. https://doi.org/10.1016/j.compscitech.2005.04.029.
[87] Bulut M, Erkliğ A. An experimental investigation on damage characteristics of laminated hybrid composites subjected to low velocity impact. Polym Compos 2018;39:3129–39. https://doi.org/10.1002/pc.24319.
[88] Safri SNA, Sultan MTH, Jawaid M, Jayakrishna K. Impact behaviour of hybrid composites for structural applications: A review. Compos Part B Eng 2018;133:112–21. https://doi.org/10.1016/j.compositesb.2017.09.008.
[89] Papa I, Formisano A, Lopresto V, Langella A. Low velocity impact behaviour of reinforced plastic laminates: Indentation and penetration laws validated for different fibres and matrices. Compos Part B Eng 2019;164:61–6. https://doi.org/10.1016/j.compositesb.2018.11.070.
[90] Evci C, Gülgeç M. An experimental investigation on the impact response of composite materials. Int J Impact Eng 2012;43:40–51. https://doi.org/10.1016/j.ijimpeng.2011.11.009.
[91] Jiang H, Ren Y, Liu Z, Zhang S, Lin Z. Low-velocity impact resistance behaviors of bio-inspired helicoidal composite laminates with non-linear rotation angle based layups. Compos Struct 2019;214:463–75. https://doi.org/10.1016/j.compstruct.2019.02.034.
[92] Ginzburg D, Pinto F, Iervolino O, Meo M. Damage tolerance of bio-inspired helicoidal composites under low velocity impact. Compos Struct 2017;161:187–203. https://doi.org/10.1016/j.compstruct.2016.10.097.
[93] Liu JL, Lee HP, Tan VBC. Failure mechanisms in bioinspired helicoidal laminates. Compos Sci Technol 2018;157:99–106. https://doi.org/10.1016/j.compscitech.2018.01.033.
[94] Crupi V, Epasto G, Guglielmino E. Internal Damage Investigation of Composites Subjected to Low-Velocity Impact. Exp Tech 2016;40:555–68. https://doi.org/10.1007/s40799-016-0057-1.
[95] Sy BL, Fawaz Z, Bougherara H. Damage evolution in unidirectional and cross-ply flax/epoxy laminates subjected to low velocity impact loading. Compos Part A Appl Sci Manuf 2018;112:452–67. https://doi.org/10.1016/j.compositesa.2018.06.032.
[96] Sayer M, Bektaş NB, Sayman O. An experimental investigation on the impact behavior of hybrid composite plates. Compos Struct 2010;92:1256–62. https://doi.org/10.1016/j.compstruct.2009.10.036.
[97] Enfedaque A, Molina-Aldareguía JM, Gálvez F, González C, Llorca J. Effect of glass fiber hybridization on the behavior under impact of woven carbon fiber/epoxy laminates. J Compos Mater 2010;44:3051–68. https://doi.org/10.1177/0021998310369602.
[98] Ghelli D, Minak G. Low velocity impact and compression after impact tests on thin carbon/epoxy laminates. Compos Part B Eng 2011;42:2067–79. https://doi.org/10.1016/j.compositesb.2011.04.017.
[99] Sutherland LS, Guedes Soares C. The use of quasi-static testing to obtain the low-velocity impact damage resistance of marine GRP laminates. Compos Part B Eng 2012;43:1459–67. https://doi.org/10.1016/j.compositesb.2012.01.002.
[100] Palomba G, Epasto G, Crupi V, Guglielmino E. Single and double-layer honeycomb sandwich panels under impact loading. Int J Impact Eng 2018;121:77–90. https://doi.org/10.1016/j.ijimpeng.2018.07.013.
[101] Abrate S, Epasto G, Kara E, Crupi V, Guglielmino E, Aykul H. Computed tomography analysis of impact response of lightweight sandwich panels with micro lattice core. Proc Inst Mech Eng Part C J Mech Eng Sci 2018;232:1348–62. https://doi.org/10.1177/0954406218766383.
[102] Crupi V, Kara E, Epasto G, Guglielmino E, Aykul H. Prediction model for the impact response of glass fibre reinforced aluminium foam sandwiches. Int J Impact Eng 2015;77:97–107. https://doi.org/10.1016/j.ijimpeng.2014.11.012.
[103] Crupi V, Kara E, Epasto G, Guglielmino E, Aykul H. Theoretical and experimental analysis for the impact response of glass fibre reinforced aluminium honeycomb sandwiches. J Sandw Struct Mater 2018;20:42–69. https://doi.org/10.1177/1099636216629375.
[104] D3822/D3822M - 14 ASTM. Standard Test Method for Tensile Properties of Single Textile Fibers.

2001.
[105] D 3039/D 3039M-00 ASTM. Standard Test Method for Tensile Properties of Polymer Matrix Composite Materials. 2002.
[106] Bongiorno F, Zuccarello B, Militello C. Analysis of the anisotropy of the agave fiber and characterization of the mechanical behavior of high performance unidirectional biocomposite lamina. Submitt Pubblication to Compos Part B Eng 2020.
[107] Aboudi J. Mechanics of composite materials. A unified micromechanical approach. Amsterdam: Elsevier Science; 1991.
[108] Ma Y, Yokozeki T, Ueda M, Sugahara T, Yang Y, Hamada H. Effect of polyurethane dispersion as surface treatment for carbon fabrics on mechanical properties of carbon/Nylon composites. Compos Sci Technol 2017;151:268–81. https://doi.org/10.1016/j.compscitech.2017.08.031.
[109] Cheng Q, Bao J, Park JG, Liang Z, Zhang C, Wang B. High mechanical performance composite conductor: Multi-walled carbon nanotube sheet/bismaleimide nanocomposites. Adv Funct Mater 2009;19:3219–25. https://doi.org/10.1002/adfm.200900663.

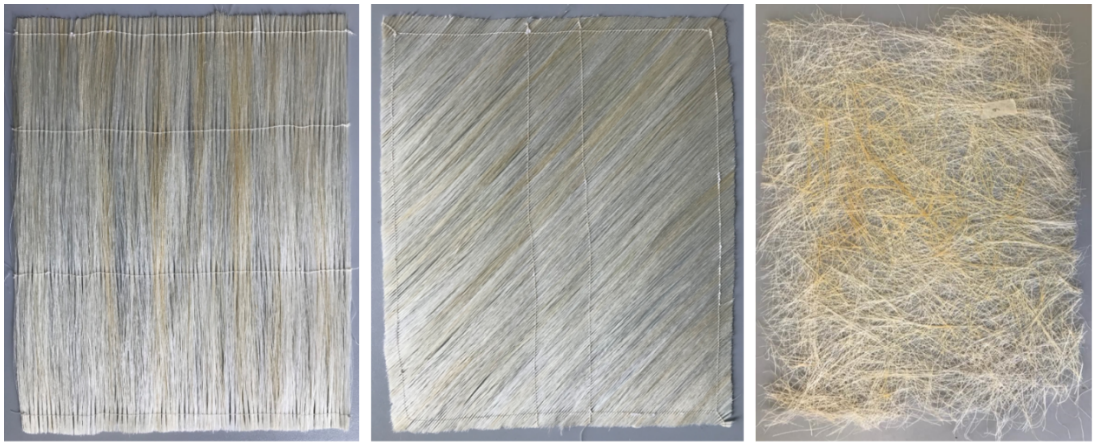

(a) (b) (c)

Fig.1 - unidirectional *stitched* fabric oriented to (a) 0° and (b) 45°, (c) MAT fabric.

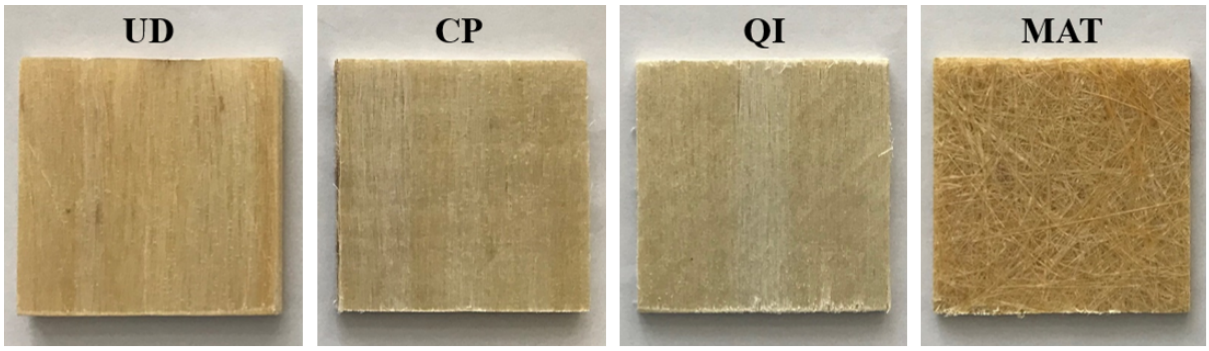

(a) (b) (c) (d)

Fig.2 – Specimens used for the impact tests: (a) unidirectional (UD), (b) cross-ply (CP), (c) quasi-isotropic (QI) and (d) MAT.

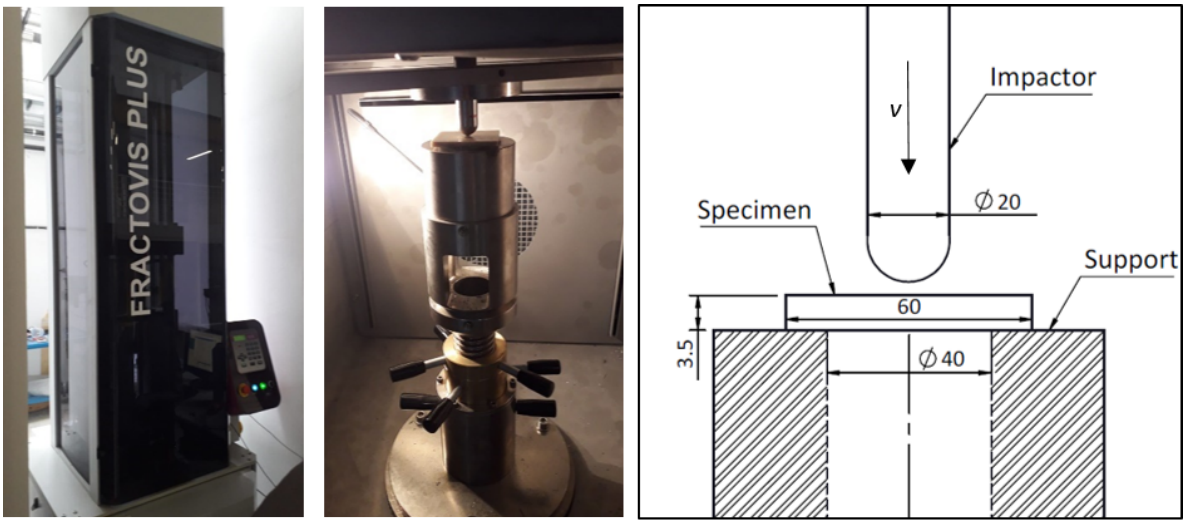

(a) (b) (c)

Fig.3 - (a) Test machine type "*Ceast Fractovis Plus*", (b) support system with impactor and (c) schematical draw.

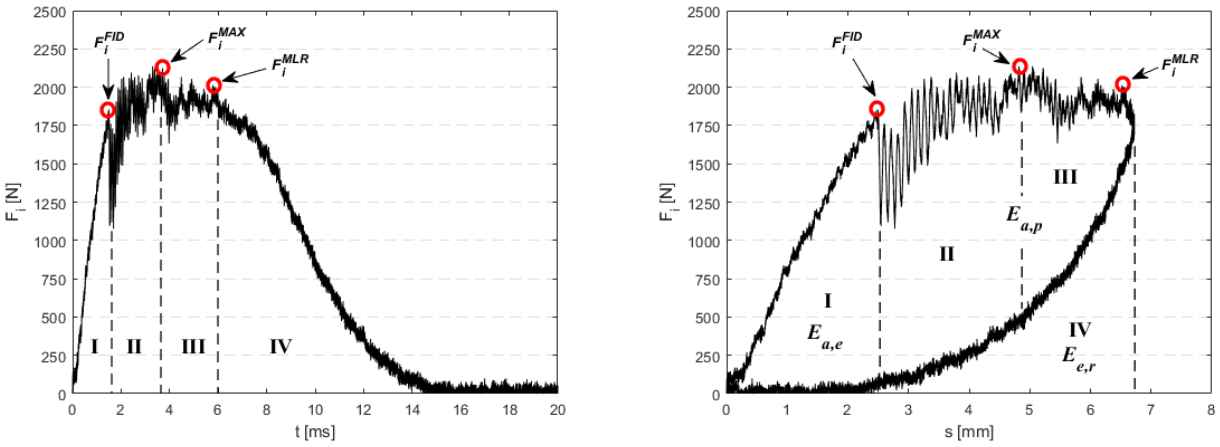

(a) (b)

Fig.4 - (a) Load-time curve and (b) load-displacement curve relative to QI biocomposite with V_f=35% and E_i =10 J.

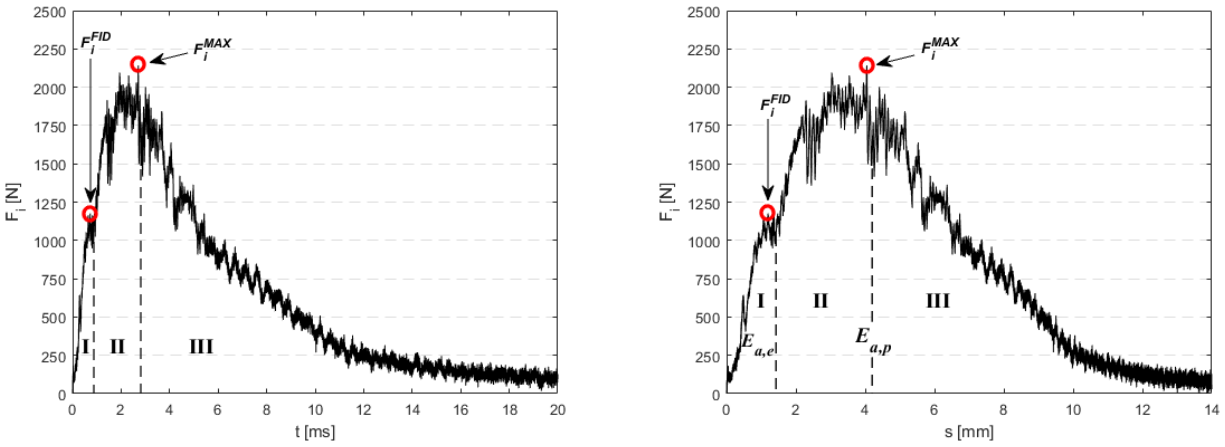

Fig.5 - (a) Load-time curve and (b) load-displacement curve relative to CP biocomposite with V_f=35% and E_i =20 J.

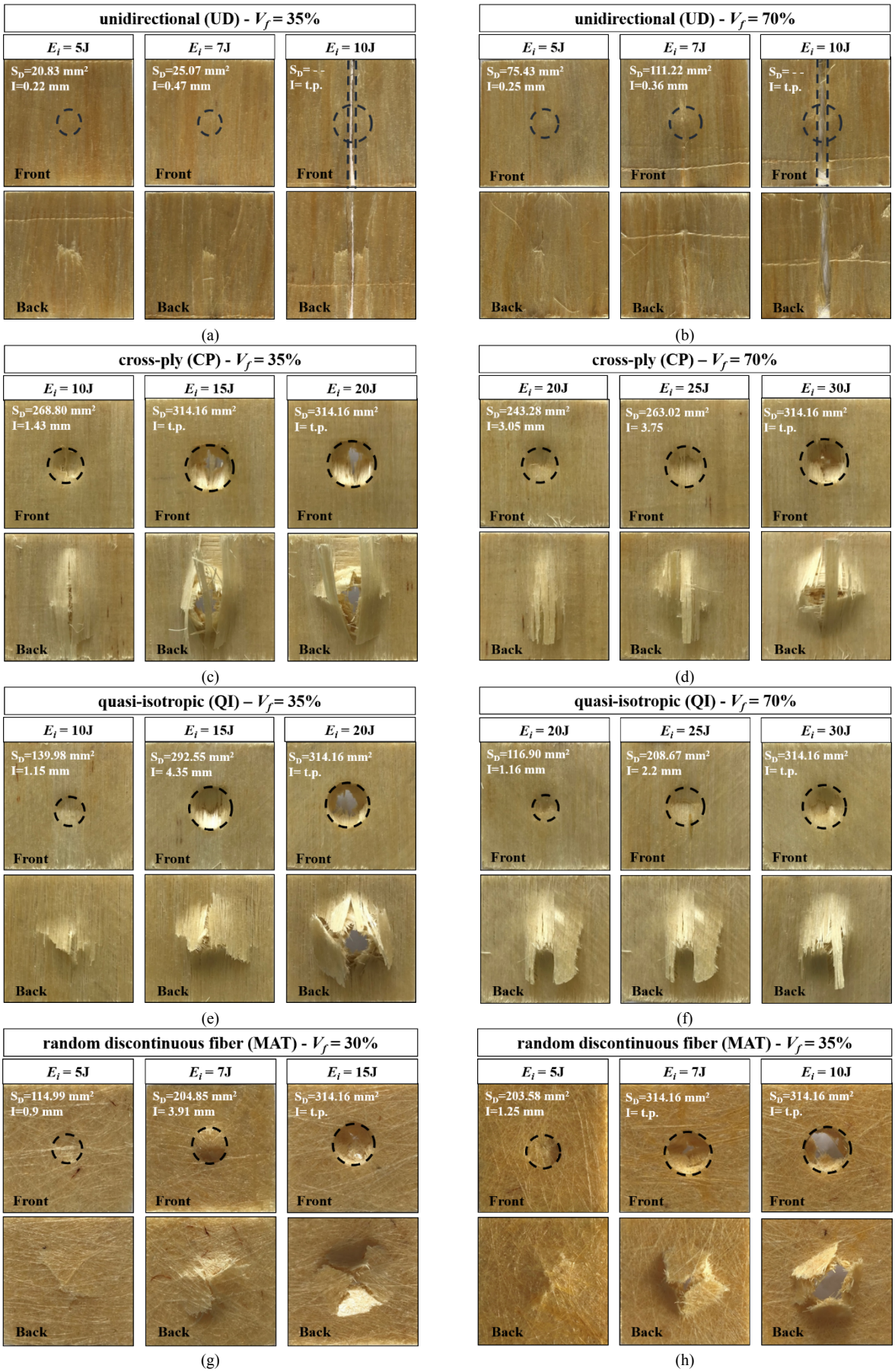

Fig.6 – Front and back view of the specimens after impact test: (a,b) unidirectional (UD), (c,d) cross-ply (CP), (e,f) quasi-isotropic (QI) and (g,h) MAT.

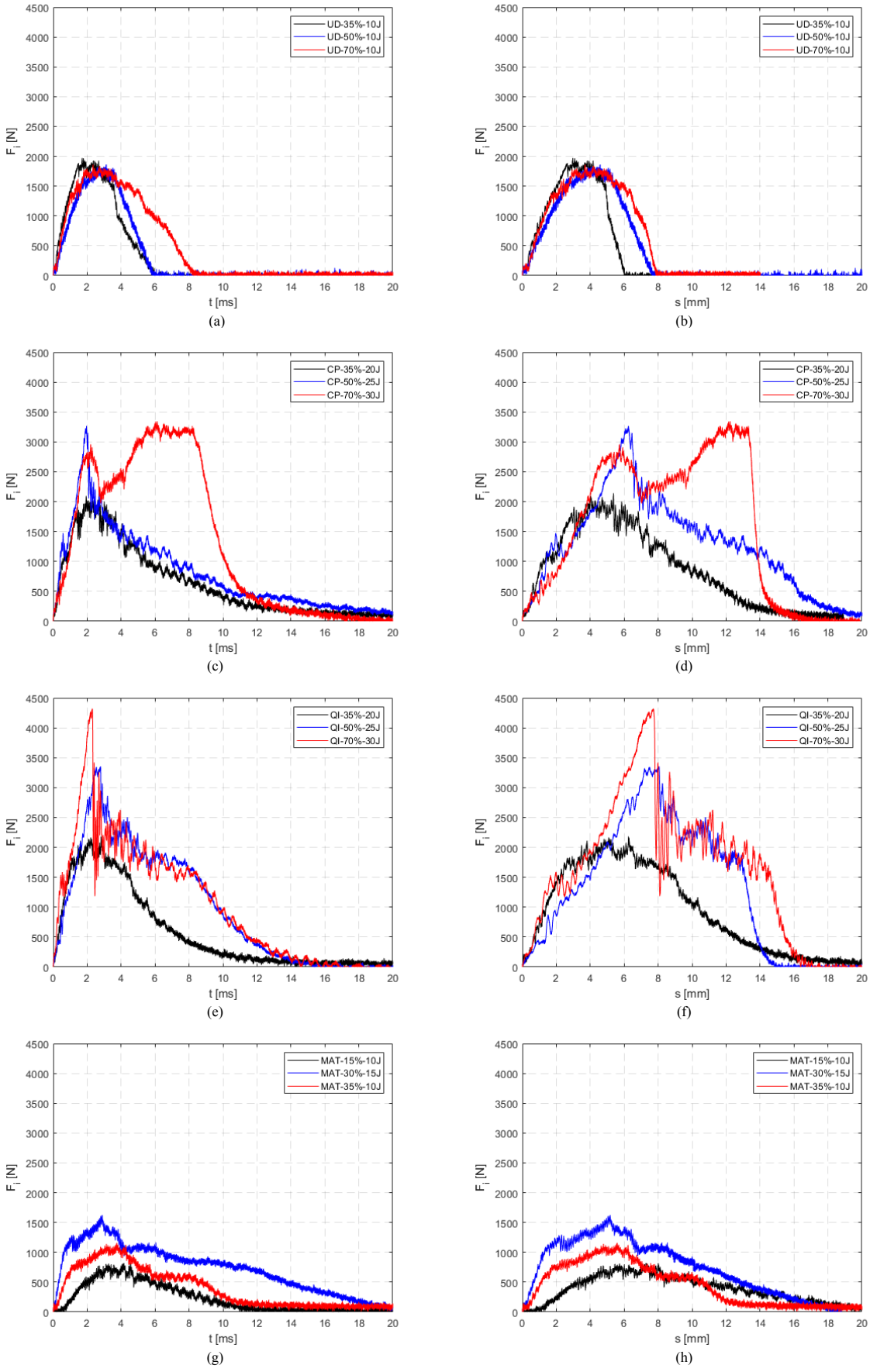

Fig.7 – Load-time and load-displacement curves for (a,b) unidirectional (UD), (c,d) cross-ply (CP), (e,f) quasi-isotropic (QI) and (g,h) MAT biocomposite laminates.

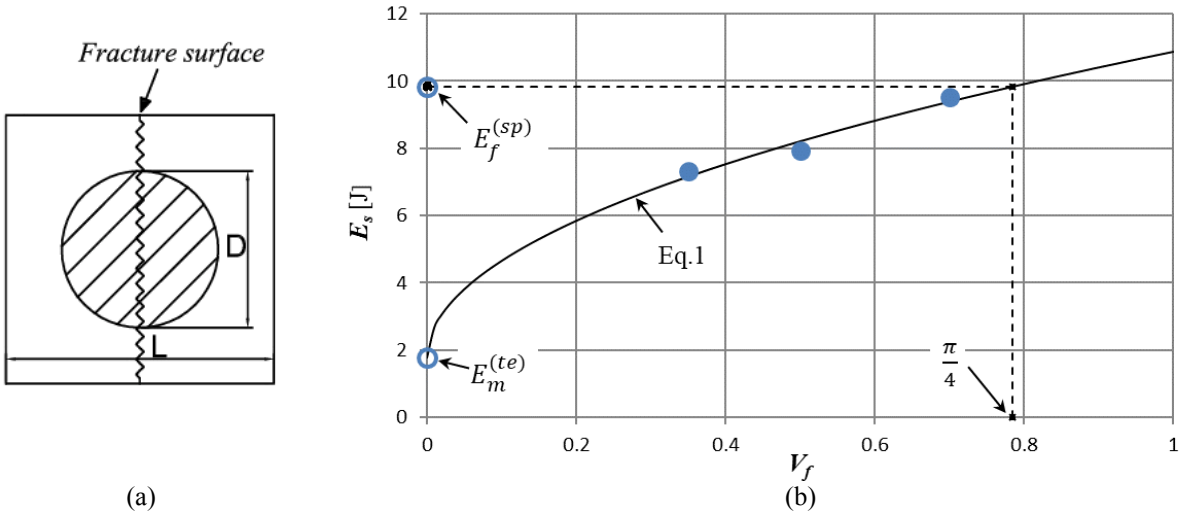

(a) (b)

Fig.8 – (a) RVE of the PMM and (b) impact strength of the unidirectional biocomposites vs. V_f and PMM model (Eq.1).

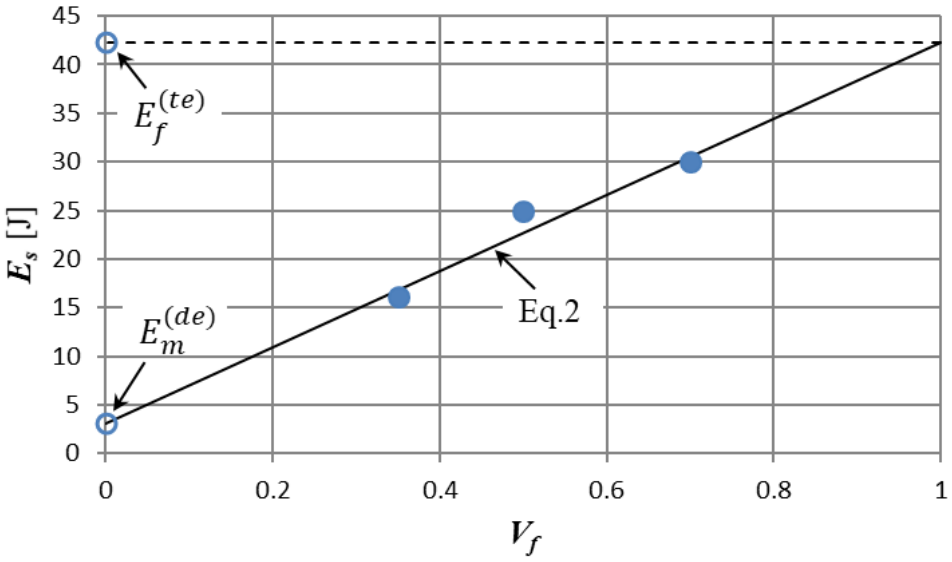

Fig.9 – Impact strength of the cross-ply (CP) biocomposites vs. V_f and ROM (Eq.2).

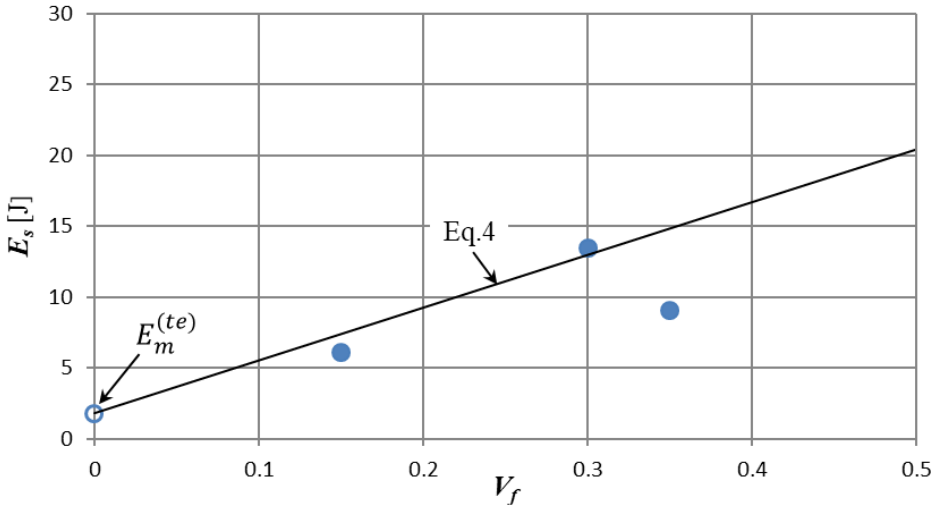

Fig.10 – Impact strength of the MAT biocomposites vs. V_f and proposed theoretical model (Eq.3) for $V_f \leq 0.3$.

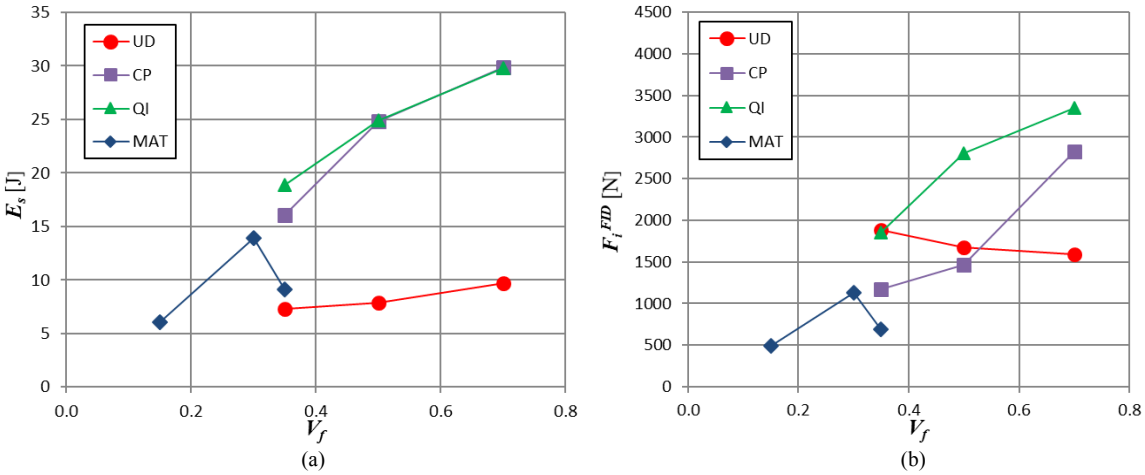

Fig.11 – (a) impact strength and (b) first impact damage force vs. V_f for the various biocomposite laminates considered.

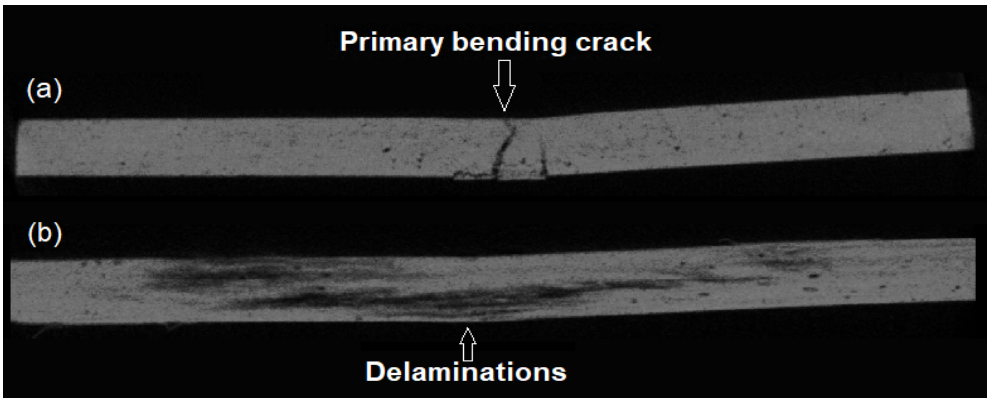

Fig.12 – X ray tomography of a tested UD specimen with V_f=35% and E_i= 7J: (a) transversal section and (b) longitudinal section.

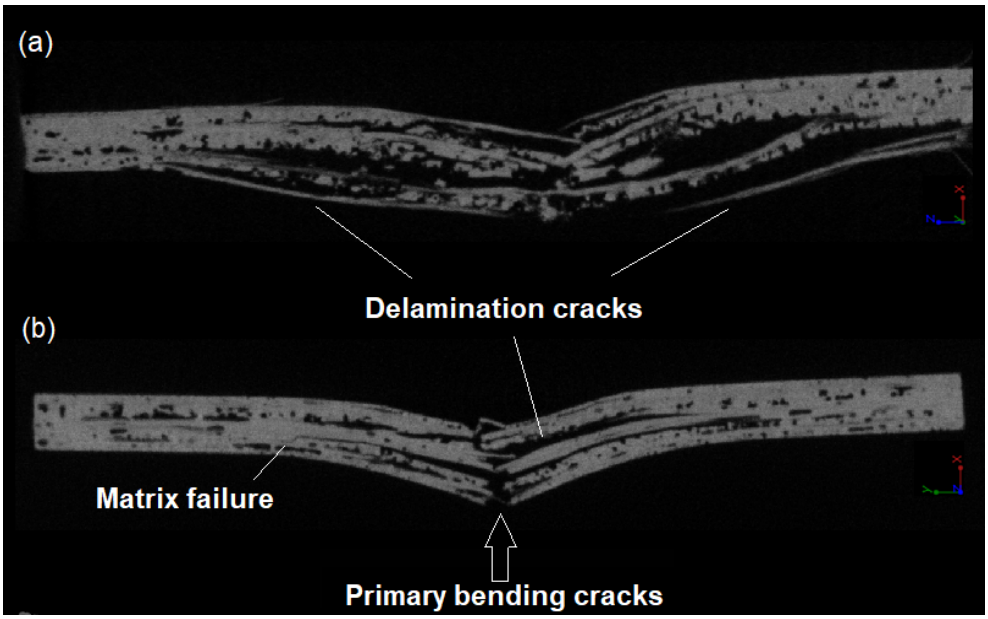

Fig.13 – X ray tomographies (a, b) of two tested CP specimens with V_f =35% ed E_i= 10 J.

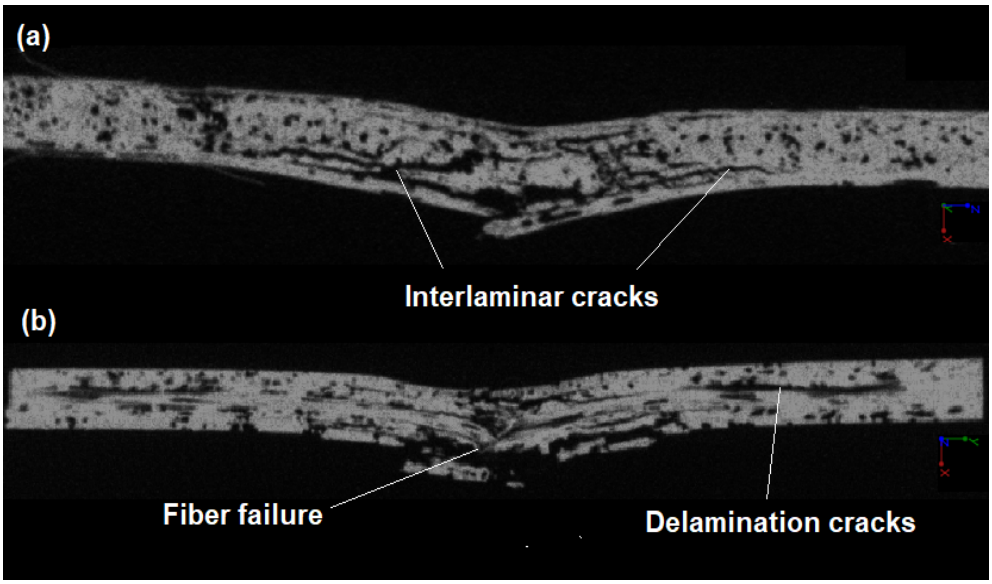

Fig.14 – X ray tomographies (a, b) of two tested QI specimens with V_f = 35% ed E_i = 10 J.

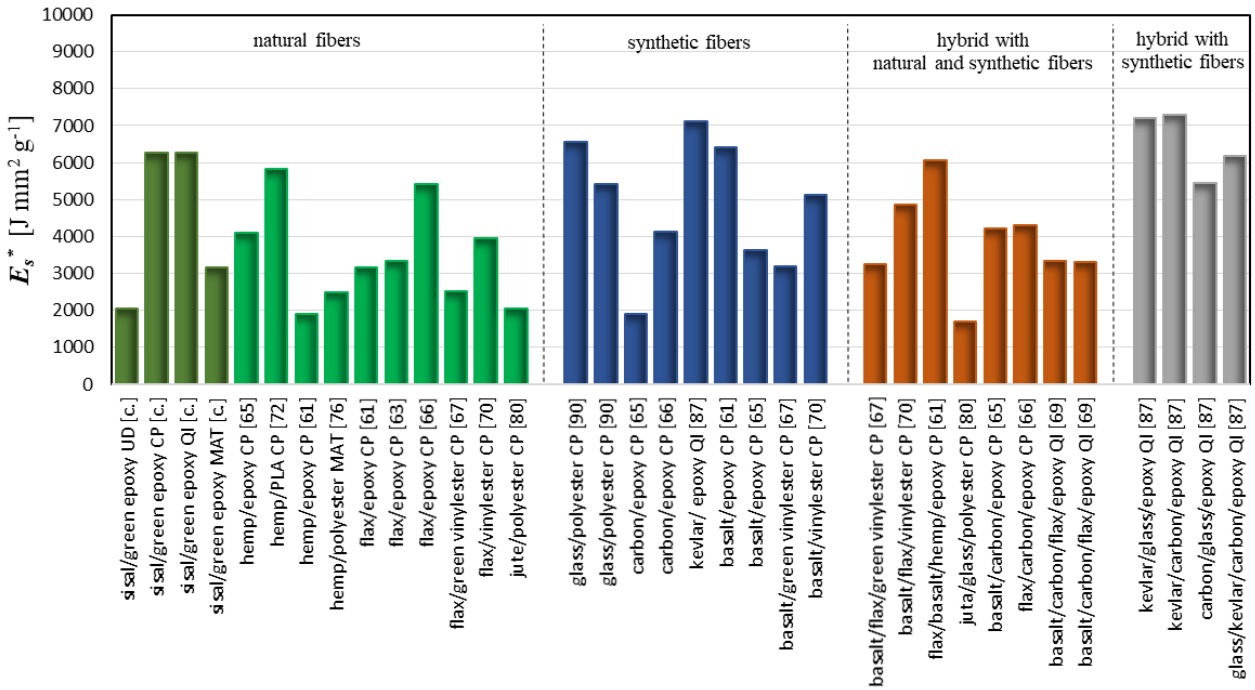

Fig.15 – Comparison of the specific impact strength of the analyzed biocomposites with that of other biocomposites and composites reported in literature.

Tab.1 – Main mechanical properties of the sisal fiber considered.

Fiber	ρ_f [g/cm^3]	$\sigma_{L,R}^{(f)}$ [MPa]	$E_L^{(f)}$ [GPa]	$\varepsilon_{L,R}^{(f)}$ [%]
Agave sisalana	1.45	685	40.50	1.75

Tab.2 – Mechanical properties of the green epoxy resin considered [51].

Matrix	ρ_m [g/cm^3]	$\sigma_{m,R}$ [MPa]	E_m [GPa]	$\varepsilon_{m,R}$ [%]	$\tau_{m,R}$ [MPa]	G_m [GPa]
Green epoxy	1.05	50	2.5	2.5	35	0.90

Tab.3 - Lay-up and fiber volume fraction of the biocomposite laminates considered.

Laminate		V_f [%]	**Lay-up**
Unidirectional	UD	35	$[0]_8$
		50	$[0]_{12}$
		70	$[0]_{16}$
Cross-ply	CP	35	$[(0/90)_2]_s$
		50	$[(0/90)_3]_s$
		70	$[(0/90)_4]_s$
Quasi-isotropic	QI	35	$[(0/\pm45/90)]_s$
		50	$[(0/\pm45/90)_3]$
		70	$[(0/\pm45/90)_2]_s$
Discontinuos fiber	MAT	15	random, 3 laminae
		30	random, 5 laminae
		35	random, 7 laminae

Tab.4 – Tensile mechanical properties of the biocomposite laminates considered.

Laminate		V_f [%]	$\sigma_{L,R}$ [MPa]	$\varepsilon_{L,R}$ [%]	E_L [GPa]
Single-layer	UD	35	230.6	1.80	16
		50	325.4	1.91	23
		70	**471.4**	**1.95**	**30**
Cross-ply	CP	35	97.7	1.40	9
		50	145.5	1.70	12
		70	**275.3**	**2.20**	**18**
Quasi-isotropic	QI	35	79.8	0.80	7
		50	96.4	1.10	9
		70	**161.5**	**1.82**	**13**
Discontinuos fibers	MAT	15	44.7	1.21	4
		30	**51.2**	**1.25**	6
		35	46.1	1.19	**7**

Tab.5 – Results of the impact tests with complete penetration (perforation) of the specimens.

Laminate		V_f [%]	E_i [J]	E_s [J]	$E_{a,e}$ [J]	$E_{a,p}$ [J]	F_i^{FD} [N]	F_i^{MAX} [N]
Unidirectional	UD	35	10	7.3	2.7	4.6	1885	2150
		50	10	7.9	2.4	5.5	1670	1860
		70	10	9.7	1.9	7.8	1590	1900
Cross-ply	CP	35	20	16.1	1.2	14.9	1175	2140
		50	25	24.8	2.4	22.6	1470	3270
		70	30	29.9	7.8	22.8	2825	3550
Quasi-isotropic	QI	35	20	18.9	3.2	15.7	1850	2180
		50	25	24.9	8.7	16.3	2800	3350
		70	30	29.8	10.8	19,2	3350	4300
Discontinuos fibers	MAT	15	10	6.1	0.5	5.6	490	810
		30	15	13.9	0.9	13.0	1135	1630
		35	10	9.1	0.6	8.5	685	1160

Tab.6 – Comparison of the specific impact strenght of the analyzed biocomposites with that of other biocomposites and composites reported in literature.

Material	Lay-up	ρ [g/cm^3]	t_s [mm]	V_f [%]	E_i [J]	E_s [J]	E_s^* [J mm^2 g^{-1}]	Rif.
Biocomposites with agave fiber (present study)								
sisal (stitched)/green epoxy	UD	1.36	3.50	70	10	9.3	1950	Current
sisal (stitched)/green epoxy	CP	1.36	3.50	70	30	30	6260	Current
sisal (stitched)/green epoxy	QI	1.36	3.50	70	30	30	6280	Current
sisal (MAT)/green epoxy	MAT	1.26	3.50	30	10	13.9	3150	Current
Biocomposites with other fibers (from literature)								
hemp (woven)/epoxy	CP	1.22	11.00	28	-	55	4090	[65]
hemp (woven)/PLA	CP	1.33	9.00	28	-	70	5840	[72]
hemp (woven)/epoxy	CP	1.17	3.70	20	-	8.2	1890	[61]
hemp (MAT)/polyester	MAT	1.40	3.00	26	-	10.5	2500	[76]
flax (woven)/epoxy	CP	1.23	3.20	24	-	12.4	3150	[61]
flax (woven)/epoxy	CP	1.3	2.97	35	15	12.9	3350	[63]
flax (pre-preg UD)/epoxy	CP	1.22	4.50	56	30	29.7	5410	[66]
flax (woven)/green vinylester	CP	1.27	6.96	57	30	22.1	2510	[67]
flax (woven)/vinylester	CP	1.20	7.10	23	36	33.6	3950	[70]
jute (woven)/polyester	CP	1.22	6.80	36	-	17	2040	[80]
Composites with synthetic fibers								
glass (woven)/polyester	CP	1.93	4.00	-	-	50.6	6550	[90]
glass (unidirectional)/polyester	CP	1.79	4.00	-	-	38.8	5420	[90]
carbon (woven)/epoxy	CP	1.38	3.50	32	12	9.2	1910	[65]
carbon (pre-preg UD)/epoxy	CP	1.40	4.50	59	30	26.0	4120	[66]
kevlar (w)/ epoxy	QI	1.29	2.70	60	-	24.8	7120	[87]
basalt (woven)/epoxy	CP	1.30	2.00	28	-	16.7	6420	[61]
basalt (woven)/epoxy	CP	1.62	3.50	32	25	20.6	3640	[65]
basalt (woven)/green vinylester	CP	1.93	3.95	49	31	24.3	3190	[67]
basalt (woven)/vinylester	CP	1.55	3.80	27	36	30.2	5130	[70]
Hybrid with natural and synthetic fibers								
basalt (w)/flax (w)/green vinylester	CP	1.38	5.38	52	34	24.2	3260	[67]
basalt (w)/flax (w)/vinylester	CP	1.30	5.10	25	36	32.3	4870	[70]
flax (w)/basalt (w)/hemp (w)/epoxy	CP	1.22	3.40	22	-	25.1	6050	[61]
juta(woven)/glass(plain)/polyester	CP	1.25	6.60	35	-	14	1690	[80]
basalt (w)/carbon (w)/epoxy	CP	1.48	3.50	32	25	21.8	4210	[65]
flax (p. UD)/carbon (p. UD)/epoxy	CP	1.38	4.50	60	30	26.8	4310	[66]
basalt (w)/carbon (w)/flax (UD)/epoxy	QI	2.21	4.00	52	38	29.4	3330	[69]
basalt (w)/carbon (w)/flax (UD)/epoxy	QI	2.21	4.00	52	38	29.2	3300	[69]
Hybrid with synthetic fibers								
kevlar (w)/glass (w)/epoxy	QI	1.39	2.70	60	-	27.0	7200	[87]
kevlar (w)/carbon (w)/epoxy	QI	1.43	2.70	60	-	28.1	7290	[87]
carbon (w)/glass (w)/epoxy	QI	1.33	2.70	60	-	23.1	5450	[87]
glass (w)/kevlar (w)/carbon (w)/epoxy	QI	1.46	2.70	60	-	24.4	6190	[87]